

The symmetric parabolic resonance

This article has been downloaded from IOPscience. Please scroll down to see the full text article.

2010 Nonlinearity 23 1325

(<http://iopscience.iop.org/0951-7715/23/6/005>)

View [the table of contents for this issue](#), or go to the [journal homepage](#) for more

Download details:

IP Address: 132.77.4.43

The article was downloaded on 13/06/2010 at 08:01

Please note that [terms and conditions apply](#).

The symmetric parabolic resonance

V Rom-Kedar^{1,3} and D Turaev^{2,4}

¹ Weizmann Institute of Science, Rehovot, 76100, Israel

² Imperial College, London, SW7 2AZ, UK

E-mail: vered.rom-kedar@weizmann.ac.il and turaev@math.bgu.ac.il

Received 21 July 2009, in final form 29 March 2010

Published 11 May 2010

Online at stacks.iop.org/Non/23/1325

Recommended by D V Treschev

Abstract

The parabolic resonance instability emerges in diverse applications ranging from optical systems to simple mechanical ones. It appears persistently in p -parameter families of near-integrable Hamiltonian systems with n degrees of freedom provided $n + p \geq 3$. Here we study the simplest ($n = 2$, $p = 1$) symmetric case. The structure and the phase-space volume of the corresponding instability zones are characterized. It is shown that the symmetric case has six distinct non-degenerate normal forms, and two degenerate ones. In the regular cases, the instability zone has the usual $O(\sqrt{\varepsilon})$ extent in the action direction. However, the phase-space *volume* of this zone is found to be polynomial in the perturbation parameter ε (and not exponentially small as in the elliptic resonance case). Finally, the extent of the instability zone in some of the degenerate cases is explored. Three applications in which the symmetric parabolic resonance arises are presented and analysed.

Mathematics Subject Classification: 37J40, 70K55, 70K70, 34C20, 34C28, 34C23

(Some figures in this article are in colour only in the electronic version)

1. Introduction

Multi-dimensional nonlinear systems, including non-integrable Hamiltonians, may have complex structures that cannot be completely classified by a finite list. Much effort is thus devoted to the study of local behaviour near specific types of orbits. In particular, in the Hamiltonian context, KAM theory and Nekhoroshev estimates may be utilized to study the

³ The Estrin Family Chair of Computer Science and Applied Mathematics.

⁴ On leave from Ben Gurion University.

local behaviour near a non-resonant torus even when the global dynamics is far from being integrable.

The study of near integrable n degrees-of-freedom Hamiltonian systems provides a complimentary strategy to the local analysis, where the global phase-space structure may be explored. Most of the integrable structures—the non-trivial level sets of the n constants of motion—are simply non-resonant tori (consider for simplicity the compact level-sets case), and by KAM theory these survive sufficiently small perturbations and are thus amenable also to the local analysis. However, other integrable structures may be destroyed by perturbations (e.g. resonant tori of various dimensions and their homoclinic or heteroclinic connections). Then, one studies the emerging phenomena that are created by generic perturbations.

One of the very basic examples is the destruction of a resonant circle, for example a circle of equilibrium states. A generic Hamiltonian perturbation destroys such a circle: only a finite number of the equilibria points persist. If the circle is normally elliptic (or normally hyperbolic), one may establish, under some non-degeneracy conditions, that a resonance zone that is normally elliptic (respectively hyperbolic) is created. The elliptic case corresponds to the extensively studied emergence of the classical resonance zone [1], whereas the normally hyperbolic case (1-saddle) has been investigated in the last two decades [17, 18]. Here we study the border-line case of a circle of equilibria which is normally parabolic.

To better understand how parabolic resonances appear in near-integrable systems, consider the following three symmetric normal forms of integrable Hamiltonians near a circle of equilibria at $I = 0$ (so (q, p, I, λ) are small):

$$H_{\text{elliptic}}(q, p, I, \varphi) = \frac{p^2}{2} + \frac{q^2}{2} + \frac{q^4}{4} + \beta \frac{(\lambda + I)^2}{2}, \quad (1.1)$$

$$H_{\text{hyperbolic}}(q, p, I, \varphi) = \frac{p^2}{2} - \frac{q^2}{2} + \frac{q^4}{4} + \beta \frac{(\lambda + I)^2}{2}, \quad (1.2)$$

$$H_{\text{parabolic}}(q, p, I, \varphi) = \frac{p^2}{2} - I \frac{q^2}{2} + \frac{q^4}{4} + \beta \frac{(\lambda + I)^2}{2}. \quad (1.3)$$

The circle of equilibria points belongs to the two-dimensional invariant manifold $\mathcal{M} = \{(q, p, I, \varphi) | I \in \mathbb{R}, \varphi \in [0, 2\pi), q = p = 0\}$. The manifold consists of normally elliptic (respectively hyperbolic) circles for the Hamiltonian H_{elliptic} (respectively $H_{\text{hyperbolic}}$) [3]. For the Hamiltonian $H_{\text{parabolic}}$ the manifold \mathcal{M} is divided into two parts: for $I > 0$ the circles are normally hyperbolic whereas for $I < 0$ the circles are normally elliptic. Such a situation, where the circle stability changes along \mathcal{M} when the action I is varied, is persistent for two-degrees-of-freedom systems [6, 19]. This situation naturally arises⁵ in modal systems and in systems for which the integrability is associated with rotational symmetry, see [33, 34, 36] and section 8.

The phase velocity on the circle $q = p = 0$ with action I is simply $\dot{\varphi}|_{q=p=0} = \beta(\lambda + I)$, so the circle with the action $I^{\text{res}} = -\lambda$ is a circle of fixed points. The appearance of such a circle is persistent in the integrable setting [21]. We call this circle resonant; In the elliptic case, each circle has two characteristic frequencies: the frequency of motion on the circle $\beta(\lambda + I)$ and the normal frequency in the qp plane. These frequencies are resonant on a countable set of I values. The circle of equilibria corresponds to the strongest possible resonance at which one of these two frequencies vanishes.

⁵ It will not, however, appear in weakly coupled product systems that are composed of one-degree-of-freedom elements.

Under sufficiently small Hamiltonian perturbations:

$$H(q, p, I, \varphi) = H_{\text{elliptic/hyperbolic/parabolic}}(q, p, I) + \varepsilon H_1(q, p, I, \varphi)$$

the hyperbolic component of \mathcal{M} persists [11], and the elliptic component persists in some averaged sense, up to exponentially small gaps [15]. In the parabolic case, these statements apply only for I values that are bounded away from zero (i.e. $|I| > \eta > 0$ provided $|\varepsilon| < \varepsilon_0(\eta)$).

Note that the motion on the perturbed manifold \mathcal{M}_ε is changed in both the elliptic and hyperbolic cases. In particular, near the circle at I^{res} , an $O(\sqrt{\varepsilon})$ region of resonance is created, where, instead of rotational circles (with $\dot{\varphi} \neq 0$ along trajectories), a region of oscillatory circles appear.

In the elliptic case, the motion normal to the manifold remains oscillatory, so the behaviour near the resonance is mostly regular: a single perturbed orbit would typically shadow a single circle belonging to the resonant structure on \mathcal{M}_ε . Chaotic orbits appear only in exponentially small bands near separatrices.

In the hyperbolic case, the hyperbolic resonance scenario creates splitting of the separatrices associated with the resonant circles, leading to the birth of infinity of transverse homoclinic orbits to these resonant circles [17, 18]. A typical trajectory thus experiences excursions along the homoclinic loop away from \mathcal{M}_ε . During these excursions the value of I may acquire an $O(\sqrt{\varepsilon})$ increment/decrement. When the orbit approaches \mathcal{M}_ε again, it shadows a resonant circle which corresponds to the new value of I . We do not know whether a typical trajectory belonging to the homoclinic tangle zone visits, when it approaches \mathcal{M}_ε , the whole resonance zone, or is it limited to shadowing only a small neighbourhood of its base limiting circle, see [33] for some simulations. One would expect that for small ε partial averaging with respect to the fast motion away from the separatrix will indeed produce KAM tori that bound the instability zone to the neighbourhood of a single circle and its separatrices.

The question addressed here is what kind of resonant behaviour one gets for the Hamiltonian system near the parabolic circle ($I = 0$) when it is nearly resonant (small λ). While we concentrate here on the two-degrees of freedom setting, this low-dimensional mechanism naturally arises when studying how higher-dimensional Hamiltonian systems transfer from a typical *a priori* stable behaviour to a system with one unstable direction (e.g. in modal systems, when one mode becomes unstable). Usually, in an integrable n degrees-of-freedom system depending on p parameters, such a transition occurs at a non-resonant $(n-1)$ -dimensional torus that is normally parabolic. Such a torus persists under small Hamiltonian perturbations [6], and the perturbed and unperturbed motions are of similar nature up to exponentially small regions of chaotic behaviour [14]. Here we are concerned with the case at which the unperturbed parabolic torus is also resonant—a persistent phenomenon for $n + p \geq 3$ [21–33]. Hence, the study may shed some light on multi-dimensional phenomenon that appear generically and can induce strong instabilities. Indeed, in a series of works [20, 35–37] it was demonstrated that parabolic resonances lead to a new type of chaotic behaviour that is distinct from the familiar homoclinic chaos: the systems exhibited a large chaotic component in which trajectories wander with long quasi-regular intervals of motion.

Here we present the theoretical justification to these claims: we analyse the behaviour near symmetric parabolic resonance and explain the observed behaviour; We find the dependence of the extent and structure of the chaotic zone on the parameters, the perturbation form and the energy. In particular, we explain why the perturbed motion in this case is drastically different from both the elliptic and hyperbolic cases: the perturbed orbits do not shadow the resonant motion on the plane \mathcal{M}_ε —instead, the trajectories wander away from \mathcal{M} and the slow variables (I, φ) follow the level lines of an adiabatic invariant J that we compute and analyse.

2. Setup

Consider a symmetric parabolic resonance Hamiltonian,

$$H_{\text{par-res}} = \frac{p^2}{2} - I \frac{q^2}{2} + \frac{q^4}{4} + \beta \frac{(\lambda + I)^2}{2} + F(p, q, I) + \varepsilon V_{\text{pert}}(q, p, I, \varphi), \quad (2.1)$$

where $\varepsilon \geq 0$ is a small parameter, $F = O(p^4 + |p^3q| + p^2q^2 + q^6 + |I|^3 + I^2q^2 + |I|p^2 + |I|pq|)$ and is an even function of (q, p) (the functions F and V_{pert} may depend on ε as well).

The Hamiltonian (2.1) _{$\varepsilon=0$} is an integrable Hamiltonian normal form near a parabolic circle of fixed points under \mathbb{Z}_2 -symmetry; we consider small (q, p, I, λ) , and will show that usually $F(q, p, I)$ may be neglected (see the scaling in section 4). The first three terms correspond to one of the symmetric normal forms near the parabolic circle at $I = 0$ [6, 16, 19]. The fourth term controls the rotation along the circle. For the regular case ($\beta \neq 0$) the unperturbed parabolic circle becomes a circle of fixed points only when $\lambda = 0$, whereas at $\lambda \neq 0$ the velocity along the parabolic circle unfolds in a transversal fashion. The behaviour near $\beta = 0$ needs a separate treatment (see section 7.2).

The Hamiltonian (2.1) produces the system:

$$\begin{aligned} \frac{dq}{dt} &= p + \varepsilon \frac{\partial V_{\text{pert}}}{\partial p} + O(|p|^3 + |p|q^2 + |Iq| + |Ip|), \\ \frac{dp}{dt} &= q(I - q^2) - \varepsilon \frac{\partial V_{\text{pert}}}{\partial q} + O(|q|^5 + |q|p^2 + |p|^3 + I^2|q| + |Ip|), \\ \frac{d\varphi}{dt} &= -\frac{q^2}{2} + \beta(\lambda + I) + \varepsilon \frac{\partial V_{\text{pert}}}{\partial I} + O(I^2 + Iq^2 + p^2 + |pq|), \\ \frac{dI}{dt} &= -\varepsilon \frac{\partial V_{\text{pert}}}{\partial \varphi}, \end{aligned} \quad (2.2)$$

which is defined on $X = (q, p, I, \varphi) \in \mathbb{R}^3 \times S^1$ and is studied at small (q, p, I, λ) . Denote by $V(\varphi) := V_{\text{pert}}(0, 0, 0, \varphi)$ the main contribution to the perturbation term at the parabolic resonance. With no loss of generality, assume

$$\max V(\varphi) = -\min V(\varphi) = 1 \quad (2.3)$$

(this is achieved by adding a constant to the Hamiltonian and by rescaling ε). Hereafter, in all the numerical demonstrations we set $V(\varphi) = \cos(\varphi)$.

The paper is ordered as follows. In section 3 we analyse the unperturbed dynamics. In section 4 we re-scale the system and bring it to a slow-fast form. We average over the fast (q, p) variables and thus define the adiabatic invariant $J(I, \varphi; H)$. We conclude that the perturbed orbits in the slow system follow the level lines of J as long as the separation of scales holds, namely as long as the separatrices in the qp plane are not crossed. In section 5 we show that while finding the level lines of J analytically is non-trivial (they are determined by elliptic integrals and depend on two variables and several parameters), much information about their structure may be extracted by utilizing a special representation of the phase space. In particular, we show in section 6 that this representation allows us to identify the shape and extent of the chaotic zone for all energy values using one planar plot. In section 7 we show that for particular singular values of β (when $\beta \in \{0, \frac{1}{2}\}$) some of the level lines of J are unbounded in I . Then, a new scaling for the instability extent emerges. In section 8 we present three applications of the parabolic resonance theory. Section 9 concludes the paper.

3. The unperturbed dynamics

Since I and H are preserved under the unperturbed Hamiltonian dynamics $(2.1)_{\varepsilon=0}$, the (q, p) -planar motion may be easily found. For $I > 0$ the phase portrait in the qp plane is of a figure-eight separatrix emanating from the origin. The separatrix width (in q) is of order \sqrt{I} and its height (in p) is of order I . For $I < 0$ the origin is a nonlinear centre.

Since for $\varepsilon \neq 0$ the motion occurs on fixed energy surfaces, to obtain information on the character of the perturbed motion, it is useful to present the unperturbed motion by its energy–momentum bifurcation diagram (EMBD). In this diagram we plot the allowed region of motion \widehat{D} in the (H, I) space. Since p^2 must be positive, it follows from (2.1) that \widehat{D} is bounded by the two parabolas $L_0 : \{H = \beta \frac{(\lambda+I)^2}{2} + o(I^2), I \in \mathbb{R}\}$ and $L_{\pm} : \{H = -\frac{I^2}{4} + \beta \frac{(\lambda+I)^2}{2} + o(I^2), I \geq 0\}$, i.e. $\widehat{D} : H \geq \beta \frac{(I+\lambda)^2}{2} - \frac{I}{4} \max\{0, I\} + o(I^2)$.

The lower half of L_0 , $L_0^- = L_0 \cap \{I < 0\}$, is a boundary of the allowed region of motion, whereas $L_0^+ = L_0 \cap \{I > 0\}$ corresponds to the separatrix set (the figure-eight level set). An energy surface is represented in this diagram by the segment (or segments): $\widehat{D}_h := \widehat{D} \cap \{H = h\}$. While the projection of an unperturbed trajectory onto the EMBD is always a single point, the projection of a perturbed trajectory (plotting $(H_0(X(t)), I(t))$ on top of the unperturbed skeleton) produces some complicated curve. Yet, as long as the perturbation term remains bounded, the projection must remain in an $O(\varepsilon)$ -neighbourhood of \widehat{D}_h . Hence, by plotting the EMBD, *a priori* rough bounds on the allowed region of motion in the perturbed system are found [22, 36]. Such bounds are independent of the KAM non-degeneracy conditions. In the phase-space regions where these are satisfied, the perturbed energy surfaces are divided by the persistent KAM tori, further restricting the range of the motion.

The energy surfaces \widehat{D}_h may be bounded or unbounded, have one connected component or two, and may or may not intersect the separatrix set L_0^+ (see figure 1). These characteristics depend on the position of L_0 and L_{\pm} . At $\beta > 1/2$ both look to the right, and so the set \widehat{D}_h is bounded and connected for all h . At $\beta \in (0, 1/2)$ the parabola L_{\pm} looks to the left, whereas L_0 is right oriented, so \widehat{D}_h is unbounded in the positive I direction, and, for $\lambda > 0$, there is a range of energies at which \widehat{D}_h has two connected components. When $\beta < 0$ both parabolas are oriented to the left, hence \widehat{D}_h is unbounded in both positive and negative I directions, and for sufficiently negative energies the energy surfaces have two connected components.

Finally, since along the curves L_0 and L_{\pm}

$$\left. \frac{dH}{dI} \right|_{L_{0,\pm}} = \frac{\partial H}{\partial I} = \frac{d\varphi}{dt}, \tag{3.1}$$

their slope determines the sign of the phase velocity along the corresponding circle. Thus, circles of fixed points appear at the folds of L_0 and L_{\pm} [33]:

$$I_{r,0} = -\lambda + o(\lambda), \quad I_{r,\pm} = \frac{\beta\lambda}{\frac{1}{2} - \beta} + o(\lambda).$$

We will see that the location of these strongly resonant circles determines the extent and geometry of the parabolic resonance instability zone. To complete the characterization of the integrable structure of the Hamiltonian system $(2.1)_{\varepsilon=0}$ we draw in figure 2 the Fomenko graphs for various intervals of energies [4, 5, 13, 32]. These graphs show how families of tori are glued together on each energy surface, or, more formally, what is the Liouville foliation of the energy surfaces. The foliation structure is determined by the curves L_0^{\pm} and L_{\pm} : at the curves L_0^-, L_{\pm} one family of tori terminates at an elliptic circle (‘atom A’ in the terminology of [12]), whereas

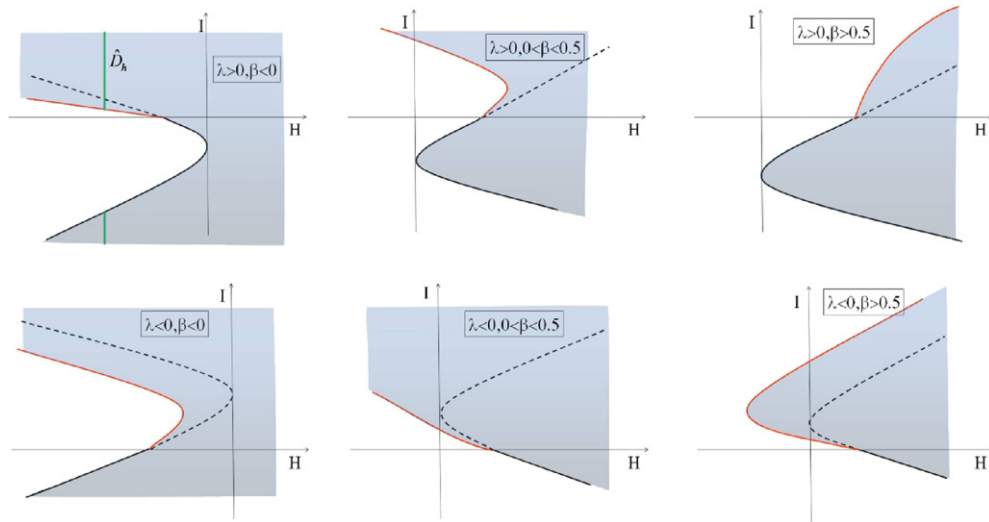


Figure 1. Six types of energy–momentum bifurcation diagrams (EMBDs) for the symmetric parabolic resonant Hamiltonian $(2.1)_{\varepsilon=0}$. Solid (dashed) curves: projections of the normally elliptic (hyperbolic) circles to the (H, I) plane. Green segments—projection of an energy surface composed of two connected components. Grey area—projection of the allowed region of motion. A point in the grey area (and not on the red/black curves) corresponds to either a torus or two disjoint tori, see figure 2.

	$\beta < 0$	$0 < \beta < 0.5$	$0.5 < \beta$
$\lambda > 0$			
$\lambda < 0$			

Figure 2. Fomenko graphs (describing the structure of iso-energetic foliation) for the six types of EMBDs, for various energy intervals. Edges correspond to families of tori, circles indicate elliptic circles (A atoms), diamonds indicate hyperbolic circles and their separatrices (B atoms).

at L_0^+ three families of tori are glued together at the figure-eight separatrix level set (‘atom B’). Here, energy surfaces with the same diagram are Liouville equivalent, and the diagrams change exactly at the folds and singularities of the curves L_0^\pm and L_\pm (in the general case more delicate issues arise [32]). Two Hamiltonian systems are called isoenergetically Liouville equivalent if the sequence of changes in their Liouville foliations is identical (see [19] for a more formal definition). Such Hamiltonians may have qualitatively similar response to small perturbations. As shown in figure 1, we have six different non-degenerate EMBDs, each corresponding to a different sequence of changes in the iso-energetic foliations:

Theorem 3.1. *At $\varepsilon = 0$ the Hamiltonian (2.1) admits six normal forms corresponding to the cases $\{\lambda > 0, \lambda < 0\} \times \{\beta < 0, \beta \in (0, 1/2), \beta > 1/2\}$. Hamiltonians belonging to the*

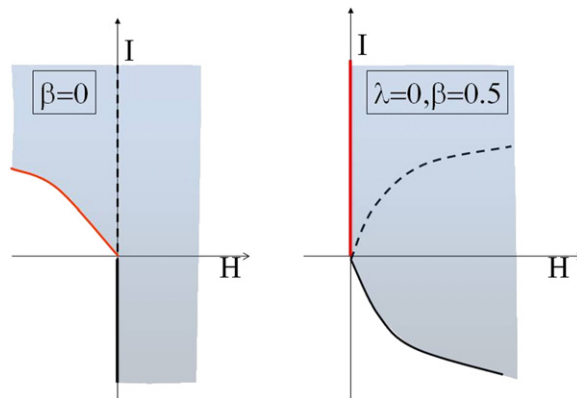


Figure 3. EMBDs at the two singular values with $F(p, q, I) \equiv 0$.

same normal form are isoenergetically Liouville equivalent, whereas Hamiltonian belonging to different normal forms are not.

Proof. Each of the six normal forms has a finite number of singular energy surfaces at which the Liouville foliation to the level sets of I are changing, and these singularities are persistent under symmetric integrable perturbations, so, near the parabolic resonance, the $F(q, p, I)$ term does not alter the structure of the foliation (see [5, 32]). The fact that these singularities and their order are unchanged in each of the equivalence classes and is different in the different classes proves this theorem. \square

The structure of the integrable system at the two singular values $\beta = 0$ and $\beta = 1/2$, $\lambda = 0$ depends on F (see section 7). When $F(q, p, I) \equiv 0$, some of the curves corresponding to families of circles become vertical rays that extend to infinity (figure 3). A vertical ray in the EMBD corresponds to the highly degenerate case of a family of circles of fixed points (see (3.1)), all residing on the same energy surface, with actions that extend to infinity. In section 7 we show that when $F(q, p, I) \equiv 0$ and $V_{\text{pert}}(q, p, I, \varphi) \equiv V(\varphi)$, these structures may produce unbounded perturbed motion.

4. The slow-fast dynamics

The behaviour near the parabolic resonance, where $(I, q, p, \lambda, \varepsilon)$ are all small, is studied by blowing up this neighbourhood to a finite size, while keeping all the four leading order terms of the unperturbed Hamiltonian (2.1). To this aim, apply the following scaling in the energy level $H_{\text{par-res}} = E$:

$$(q, p, I, \varphi, t, E, \lambda) \rightarrow (\mu q, \mu^2 p, \mu^2 I, \varphi, t/\mu, \mu^4 H, \mu^2 \Lambda), \tag{4.1}$$

where μ is some small parameter. In the new coordinates the Hamiltonian is

$$H = \frac{p^2}{2} - I \frac{q^2}{2} + \frac{q^4}{4} + \beta \frac{(\Lambda + I)^2}{2} + MV(\varphi) + \mu G(q, p, I, \varphi), \tag{4.2}$$

where $\Lambda = \lambda/\mu^2$, $M = \varepsilon/\mu^4$, $H = E/\mu^4$. The function G is uniformly bounded on any bounded phase-space region along with its derivatives. Hereafter we denote by $O(\mu)$ all the terms like μG , namely terms that remain order- μ small as long as the rescaled variables remain in a bounded region.

After the rescaling, the symplectic form becomes $dp \wedge dq + \mu^{-1}dI \wedge d\varphi$, so (φ, I) are now slow variables (velocities of order μ) and (q, p) are fast (velocities of order one):

$$\begin{aligned}\frac{dq}{dt} &= p + O(\mu), \\ \frac{dp}{dt} &= q(I - q^2) + O(\mu), \\ \frac{d\varphi}{dt} &= \mu \left(-\frac{q^2}{2} + \beta(\Lambda + I) + O(\mu) \right), \\ \frac{dI}{dt} &= -\mu(MV'(\varphi) + O(\mu)).\end{aligned}\tag{4.3}$$

The first two equations (for the frozen values of I and φ) constitute the fast subsystem. Its leading order behaviour at bounded values of the rescaled variables (p, q, I) is given by the system at $\mu = 0$:

$$\frac{dq}{dt} = p, \quad \frac{dp}{dt} = q(I - q^2).\tag{4.4}$$

This system has a Hamiltonian $H_{\text{fast}} = \frac{p^2}{2} - I\frac{q^2}{2} + \frac{q^4}{4}$. For frozen I and φ (the limit $\mu = 0$ of (4.3)), the energy of the fast motion depends on the energy h of the full system and on (I, φ) : $H_{\text{fast}} = h - \beta\frac{(\Lambda+I)^2}{2} - MV(\varphi)$.

For any $I < 0$, the origin in the qp plane is stable, and thus the rescaled qp motion corresponds to fast oscillations around the origin. For $I > 0$, the origin in the qp plane is a saddle, and two stable equilibria appear at $q = \pm\sqrt{I}$. In this case, at $H_{\text{fast}} < 0$, the motion in the qp -plane corresponds to fast oscillations around the centres at $\pm\sqrt{I}$, while at $H_{\text{fast}} > 0$ we have fast oscillations surrounding the figure-eight separatrices of the saddle at the origin.

Define the *action* $J(I, \varphi; h)$ as the area (at $\mu = 0$) of the region $H(q, p, I) \leq h$ in the (q, p) -plane for the given value of (I, φ) :

$$J(\varphi, I) = 2\sqrt{2} \int_{q_-}^{q_+} \sqrt{h - MV(\varphi) - \frac{\beta}{2}(I + \Lambda)^2 - \frac{q^4}{4} + I\frac{q^2}{2}} dq,$$

where q_{\pm} are set so that J is continuous across the separatrix set

$$S(h) := \left\{ (\varphi, I) \mid h = \beta\frac{(\Lambda + I)^2}{2} + MV(\varphi) \right\}$$

(this is the set $H_{\text{fast}} = 0$, the equivalent of L_0^+ , see section 5).

A standard application of the adiabatic invariant theorem [1, 23] implies: *for any m , there exists a function $J_m(I, \varphi; \mu) = J(I, \varphi) + O(\mu)$ such that for all small μ , for any orbit $(q(t), p(t), I(t), \varphi(t))$ of the full system, the value of $J_m(I(t), \varphi(t); \mu)$ remains $O(\mu^m)$ close to its initial value on a time interval of length $O(\mu^{-m})$, provided the orbit stays bounded away from the separatrix set.*

The slow dynamics on the energy surface h (in some rescaled time) is, up to $O(\mu)$ -terms, given by

$$\varphi' = \frac{\partial J(\varphi, I; h)}{\partial I}, \quad I' = -\frac{\partial J(\varphi, I; h)}{\partial \varphi}.\tag{4.5}$$

The slow variables follow the level lines of J until they hit the separatrix set $S(h)$. Then, adiabaticity no longer holds, and the value of J may jump to any other value between $J_{\min}(h) = \min\{J(I, \varphi, h) \mid (I, \varphi) \in S(h)\}$ and $J_{\max}(h) = \max\{J(I, \varphi, h) \mid (I, \varphi) \in S(h)\}$

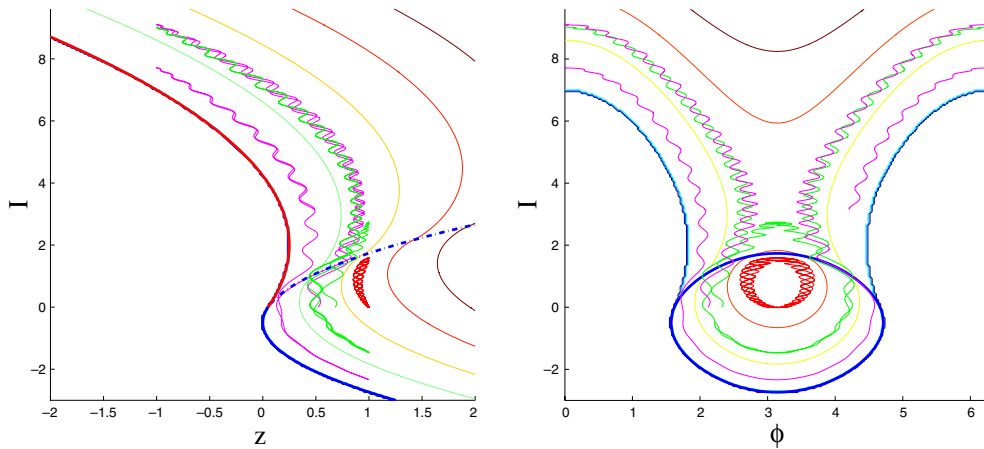


Figure 4. Three perturbed trajectories (green, red and magenta curves) are projected to the modified energy–momentum diagram (left) and to the rescaled slow-variables plane (right). The J level lines are drawn for reference (thin coloured lines). Trajectories follow the J level lines as long as they are bounded away from the separatrix set (the thick dashed blue curve). At the separatrix the J levels are changing (green and magenta orbits). Trajectories that start at a J level that does not cross L_0^+ remain regular (red orbit). Here $\beta = 0.4$, $\varepsilon = 0.01$, $\lambda = 0.05$, $H = 0$.

(see figure 4). Indeed, the saddle equilibrium of the fast subsystem corresponds to a two-dimensional (parametrized by (I, φ)) normally hyperbolic invariant manifold \mathcal{M}_+ of the full system. The stable and unstable manifolds of \mathcal{M}_+ are approximated by the fast separatrices of the saddle, so hitting $S(h)$ means coming close to the stable manifold of \mathcal{M}_+ ; the orbits that come close to the stable manifold may stay near \mathcal{M}_+ for an arbitrarily long time until exiting near some orbit of the unstable manifold; this orbit corresponds to a new value of $(I, \varphi) \in S(h)$, and the new value of $J(I, \varphi)$ may, in principle, be any number between $J_{\min}(h)$ and $J_{\max}(h)$. The separatrix crossing map provides a detailed characterization of the changes in the functions $J_m(I, \varphi)$ at the separatrix set and usually shows that J_m undergo essentially random jumps, typically of order $O(\mu)$ [9, 10, 24, 25, 40].

We conclude that the plane of the rescaled (I, φ) (more precisely—the region $D(h)$ of the allowed motion in this plane defined by $h - \beta \frac{(\Lambda + I)^2}{2} - MV(\varphi) \geq \min_{p,q} H_{\text{fast}} = -\frac{1}{4} \max(0, I)$), is divided into two regions:

Regular zone. The union of all the level lines of $J(I, \varphi; h)$ that do not intersect the separatrix set $S(h)$.

Instability/chaotic zone. The union of all the J level lines that intersect the set $S(h)$.

These zones are defined by the properties of the limiting slow system. In particular, there are a finite number of limiting J level sets that define the boundary between the two regions. For small μ , the interior part of the regular zone is mainly occupied by KAM tori that are $O(\mu)$ -close to the level lines of J and the perturbed motion stays near these tori forever [1]. On the other hand, the perturbed motion in the instability zone consists of a drift along the J level lines interrupted by jumps near the separatrix set as described above. The boundary level lines (that belong to the regular set and are close to $S(h)$) are also destroyed. Namely, the perturbed boundary between the regular and the chaotic regions is close but does not coincide with the boundary between the chaotic and regular zones of the limit system. This is the typical scenario of adiabatic chaos [9, 10, 24, 25, 40].

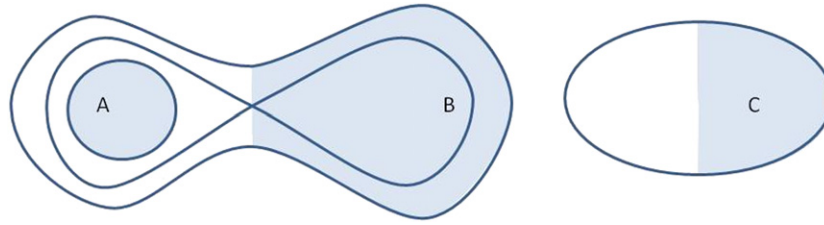


Figure 5. The definition of a continuous action. The shaded area is $J(z, I)$, where $z = H_f + \frac{1}{2}\beta(I + \Lambda)^2$, for: A: $I > 0, H_f < 0$, B: $I > 0, H_f > 0$, C: $I < 0, H_f > 0$.

We emphasize that these definitions must be interpreted in the usual mixed phase-space Hamiltonian context: at $\mu \neq 0$ within the regular zone there are exponentially small resonance regions with chaotic trajectories between KAM tori; within the chaotic zone there are islands of stability, whose total area on the cylinder of the rescaled (I, φ) variables may remain bounded away from zero as $\mu \rightarrow 0$ [9, 27, 29, 30]); Nonetheless, the orbits in the regular and the chaotic zones exhibit quite distinct motion patterns.

We will show that both the regular and the chaotic zones on the cylinder of the (rescaled) (I, φ) -variables are non-empty and their area and size remain bounded away from zero for a range of energy values. We will also show that at $\beta \neq 0$ and $\beta \neq 1/2$ the size of the chaotic zone is bounded from above.

5. The level sets of the adiabatic invariant

A priori, one may think that classifying all possible behaviours for the various forms of the level sets of J and of the separatrix set is an impossible task—the dependence on β, Λ, h, M, V appears to be overwhelming. Note, however, that $J(I, \varphi; h)$ depends on φ, h, M through the single combination $z := H - MV(\varphi)$:

$$J(z(\varphi; h), I; \beta, \Lambda) = 2\sqrt{2} \int_{q_-}^{q_+} \sqrt{z - \frac{\beta}{2}(I + \Lambda)^2 - \frac{q^4}{4} + I \frac{q^2}{2}} dq, \quad (5.1)$$

$$q_{\pm} = \sqrt{I \pm \sqrt{I^2 + 4z - 2\beta(I + \Lambda)^2}} \quad \text{for } I > 0, z - \frac{1}{2}\beta(I + \Lambda)^2 \in (-\frac{1}{4}I^2, 0),$$

$$q_- = 0, \quad q_+ = \sqrt{I + \sqrt{I^2 + 4z - 2\beta(I + \Lambda)^2}} \quad \text{for } I \in \mathbb{R}, z > \frac{1}{2}\beta(I + \Lambda)^2,$$

where we choose q_{\pm} so that $J(z, I)$ is continuous (see figure 5) across the separatrix set $S := \{(z, I) \mid z(I) = \beta \frac{(\Lambda + I)^2}{2} \text{ and } I \geq 0\}$.

Next, we show that it is possible to gain qualitative insights regarding the structure of the level sets of J in the (z, I) plane for arbitrary h value. Then, we show that the level sets of J in the (φ, I) plane on a given energy level h may be readily found from the level sets presentation in the (z, I) plots.

5.1. The level lines in the (z, I) plane

For all bounded I , the boundary of the allowed region of motion in the (z, I) plane is simply (see, e.g. (5.1)):

$$D : z(I) \geq \beta \frac{(I + \Lambda)^2}{2} - \frac{I}{4} \max\{0, I\}. \quad (5.2)$$

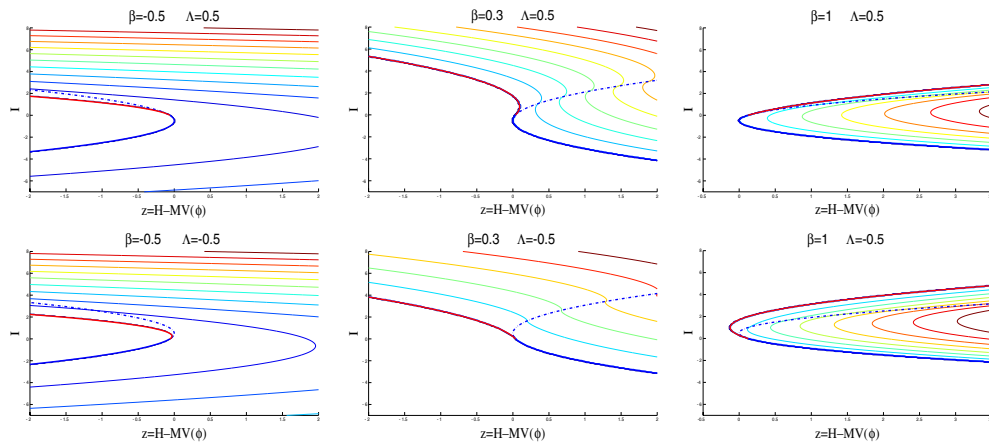


Figure 6. J level sets for the six regular β -values cases. The dashed blue line shows the separatrix set. The thick solid red and blue lines show the $J = 0$ level set. The thin coloured curves show the positive J level sets.

From (5.1) and (5.2) we immediately conclude:

Lemma 5.1. *The function $J(z, I)$ defined by (5.1) has the following properties:*

- J is smooth for all (z, I) that are bounded away from the separatrix set.
- $J(z, I) = 0$ if and only if (z, I) belongs to $\partial_L D$, the left boundary of D : $\partial_L D = \{I < 0, z = \frac{1}{2}\beta(I + \Lambda)^2\} \cup \{I \geq 0, z = \frac{1}{2}\beta(I + \Lambda)^2 - \frac{1}{4}I^2\}$.
- $J(z, I)$ is monotonically increasing in z : $\frac{\partial J}{\partial z} > 0$ in $D \setminus S$.

Corollary 5.2. *For sufficiently small j , for I values that are bounded away from 0, the level set $J(z, I) = j$ is C^1 -close to $\partial_L D$.*

The level sets of $J(z, I)$ for the six non-degenerate cases shown in figure 1 are found numerically and are shown for a few representative values in figure 6. Notice the similarity of these figures to the EMBD of the unperturbed dynamics shown in figure 1. This is not accidental: if we set $\varepsilon = 0$ in (2.1) and drop the higher order terms (set $F(q, p, I) \equiv 0$), we obtain equation (4.2) where H in the former equation is replaced by z in the latter one⁶. Thus, the boundary $\partial_L D$ in the (z, I) plane corresponds exactly to the union of the curves L_0^- and L_{\pm} of the EMBD in the (H, I) space, i.e. the unperturbed EMBDs of the normal form (2.1) provide a ‘skeleton’ for the J level lines at small J . Next, we prove that for all regular values of β , for large I values, the level sets look essentially horizontal. Then, we show that this property may be utilized to obtain bounds on the perturbed instability zone.

Since $\frac{\partial J}{\partial z} \neq 0$, the level sets of $J(z, I) = j$ are always graphs $z = z_j(I)$, $I \in \mathbb{R}$. Recall that by (2.3) and z definition, the allowed region of motion in the (z, I) plane on a given energy surface H is given by

$$D_H := D \cap \{z \in [H - M, H + M]\}. \tag{5.3}$$

Thus, on a given energy surface, these level sets of J appear as segments $Z_{j,H}$ that correspond to the intersection of the curve $z = z_j(I)$ with the strip $z \in [H - M, H + M]$. Next, we

⁶ If higher order terms were included in the system, such statement would have been correct only locally, for sufficiently small I values. See section 8.3 for an example in which the EMBD of the full system is not identical to the local one.

establish that in the non-degenerate cases, i.e. for $\beta \neq 0, 1/2$, the segments $Z_{j,H}$ must be bounded in I . First, we note that it follows from equations (5.2) and (5.3) that for $\beta > 1/2$ for any H the strip D_H is restricted to finite I values, hence all the curves $Z_{j,H}$ are indeed bounded in I . For $\beta < 1/2$ the strip D_H is unbounded: at $\beta \in (0, 1/2)$ it is a semi-infinite strip (the energy surface is bounded from below, see (5.2) and figure 1), whereas at $\beta \in (-\infty, 0)$ it is an infinite strip. Still, the boundedness of $Z_{j,H}$ immediately follows from the proposition below (since the level sets cannot intersect each other).

Proposition 5.3. *At large j , if $\beta < 0$ or $\beta \in (0, 1/2)$, the segments $Z_{j,H}$ are close to horizontal straight lines: $I(z) = c + O(j^{-2/3})$ where the constant c is $O(j^{2/3})$.*

Proof. For large $|I|$ values (in particular for $I \neq 0$), rewrite (5.1), by substituting $x = q/\sqrt{|I|}$, to obtain

$$\begin{aligned}
 J(z, I; \beta, \Lambda) &= \sqrt{8}|I|^{3/2} \int_{x_-}^{x_+} \sqrt{\frac{z - \frac{\beta}{2}(I + \Lambda)^2}{I^2} + \text{sign}(I)\frac{x^2}{2} - \frac{x^4}{4}} \, dx \\
 &= \sqrt{8}|I|^{3/2} K\left(\frac{z - \frac{\beta}{2}(I + \Lambda)^2}{I^2}, \text{sign}(I)\right).
 \end{aligned}
 \tag{5.4}$$

This defines two functions, $K(h, \pm)$, that may be expressed in terms of elliptic integrals. The function $K(h, -)$ is defined for $h \geq 0$, is smooth, vanishes at $h = 0$ and is strictly positive and increasing for $h > 0$. The function $K(h, +)$ is defined for $h \geq -1/4$, it is smooth for $h \neq 0$, vanishes at $h = -1/4$, is strictly positive and increasing for $h > -1/4$, and $\sqrt{8}K(0, +) \approx 1.333\dots$. In the limit of large $|I|$, if $\beta \in (-\infty, 0) \cup (0, 1/2)$ we expand the above expression to obtain

$$J(z, I; \beta, \Lambda) = \sqrt{8}|I|^{3/2} K\left(-\frac{\beta}{2}, \text{sign}(I)\right) \left(1 - \frac{\beta\Lambda}{I} \frac{K'\left(-\frac{\beta}{2}, \text{sign}(I)\right)}{K\left(-\frac{\beta}{2}, \text{sign}(I)\right)} + O\left(\frac{z}{I^2}\right)\right).$$

It follows that for sufficiently large j the level set $J(z, I; \beta, \Lambda) = j$ is given by

$$\begin{aligned}
 |I| &= \left(\frac{j}{\sqrt{8}K\left(-\frac{\beta}{2}, \text{sign}(I)\right)}\right)^{2/3} + \text{sign}(I)\frac{2}{3}\beta\Lambda \frac{K'\left(-\frac{\beta}{2}, \text{sign}(I)\right)}{K\left(-\frac{\beta}{2}, \text{sign}(I)\right)} \\
 &\quad + O\left(\left(\frac{j}{K\left(-\frac{\beta}{2}, \text{sign}(I)\right)}\right)^{-2/3} z\right).
 \end{aligned}$$

Thus, if $\beta < 0$, the level set is $O(j^{-2/3})$ close to the two horizontal lines:

$$I_{\pm}(z) = \frac{1}{2K\left(-\frac{\beta}{2}, \pm\right)^{2/3}} j^{2/3} \pm \frac{2}{3}\beta\Lambda \frac{K'\left(-\frac{\beta}{2}, \pm\right)}{K\left(-\frac{\beta}{2}, \pm\right)} + O\left(\frac{z}{j^{2/3}}\right), \quad |z - H| \leq M,
 \tag{5.5}$$

whereas if $\beta \in (0, 1/2)$, the level set consists of only the upper curve $I_+(z)$. The z dependence of $I_{\pm}(z)$ enters only in the correction term. \square

Since the curves $Z_{j,H}$ are bounded in I , each segment $Z_{j,H}$ is defined on a finite interval $[I_{\min}(j, H), I_{\max}(j, H)]$ and $z_j(I_{\min, \max}) = H \pm M$. We say that $Z_{j,H}$ is horizontal if it extends across the energy strip, namely $z_j(I_{\min}) \neq z_j(I_{\max})$, and vertical if it does not, namely $z_j(I_{\min}) = z_j(I_{\max})$. The vertical curves are necessarily non-monotone, and the horizontal curves can be either monotone ($z'_j(I) \neq 0$ for all $I \in [I_{\min}(j, H), I_{\max}(j, H)]$) or not. Proposition 5.3 shows that in the non-degenerate cases, for sufficiently large $|I|$, all the level segments are horizontal and monotone.

5.2. The slow-variables phase space

The structure of the level lines of $J(\varphi, I, H) = j$ can be easily read off from the properties of the curves $Z_{j,H}$. Denote by $\varphi_{j,H}$ the pre-image of the curve $Z_{j,H}$ in the (φ, I) phase space. Recall that J may be regarded as a Hamiltonian for the slow-variables dynamics (equation (4.5)). Note that $\nabla_{\varphi, I}(J) = (-MV'(\varphi) \frac{\partial J}{\partial z}, \frac{\partial J}{\partial I})$, recall that $\frac{\partial J}{\partial z} > 0$ and that $z'_j(I) = -\frac{\partial J}{\partial I} / \frac{\partial J}{\partial z}$. Thus, a reversal of the flow direction in φ occurs exactly at extremal points of $z_j(I)$, and similarly, reversal of motion in I occurs only at extremal points of V . Hence, horizontal segments typically correspond to rotational motion in the (φ, I) coordinate system whereas the vertical segments correspond to the oscillatory regime.

The singular level curves that contain fixed points of the slow dynamics may occur only at non-monotone curves for specific energy values. These can be found from the level plots of J in the (z, I) plane; Let I_e denote an extremal point of a component of the j level set $z = z_j(I)$, so that $z'_j(I_e) = 0$, and let φ_e be an extremal point of $V(\varphi)$. Since $(\varphi', J') = (\frac{\partial J}{\partial I}, MV'(\varphi) \frac{\partial J}{\partial z})$, on the energy surfaces $H = z_j(I_e) + V(\varphi_e)$ the j level set has a singular component $\varphi_{j,H}$ and the slow dynamics has a fixed point at (φ_e, I_e) . The eigenvalues of (φ_e, I_e) are $\rho^2 = M \frac{\partial^2 J}{\partial I^2} V''(\varphi) \frac{\partial J}{\partial z}$, and thus the fixed point is a saddle (and then the $\varphi_{j,H}$ component is non-trivial) if $MV''(\varphi_e) \frac{\partial^2 J}{\partial I^2} > 0$ and a centre if the opposite inequality occurs. In particular, the segments that are tangent to the bounding vertical lines $z = H \pm M$ are singular, since they contain stagnation points.

Combining proposition 5.3 and the above observations we arrive at:

Proposition 5.4. For $\beta \neq 0, \frac{1}{2}$, for all H values with non-trivial D_H , for all j values with the exception of a finite number of values j_{sin} , the level sets $\Phi(j, H) : \{J(I, \varphi) = j\}$ are composed of circles in the (I, φ) cylinder. Moreover, for all sufficiently large $|I|$ these circles embrace the cylinder and are bounded away from the separatrix set S .

Proof. Note that we only need to prove the last statement. Indeed, it implies that the level sets of J are bounded in I , so the level sets must be closed non-intersecting curves, and hence only at a finite number of values these level sets can degenerate to points or to (slow) separatrices.

If D_H is unbounded, then proposition 5.3 shows that the corresponding curves $Z_{j,H}$ are monotone horizontal and bounded, hence for sufficiently large $|I|$ these circles embrace the cylinder and satisfy $I(\varphi) = c(j) + O(j^{-2/3})$, where $c(j) = O(j^{2/3})$ is independent of φ . Note that the j level sets that cross the separatrix set S satisfy (use $z \in [H - M, H + M]$, $z_{\text{sep}} = \frac{\beta}{2}(I + \Lambda)^2$ and (5.4)):

$$2(H - M) \leq \beta \left(\left(\frac{j}{\sqrt{8K(0, +)}} \right)^{2/3} + \Lambda \right)^2 \leq 2(H + M), \tag{5.6}$$

which shows that the values of j on S are bounded from above, so the level sets which correspond to large j —hence to large $|I|$ —do not intersect S .

If the energy surface is bounded, then, in the (z, I) plane it is bounded by the segments $Z_{j=0,H} = \partial_L D \cap [H - M, H + M]$, the intersection of the $j = 0$ level lines with the energy strip. The level lines with small j are C^1 -close to this bounding surface (see corollary 5.2). These can correspond to large I values only when $|H|$ is large. Indeed, for sufficiently large $|H|$ and $\beta \neq 0, 1/2$ this segment is clearly horizontal, and by (5.6) the small j level sets are indeed bounded away from the separatrix set. \square

The above proposition shows that at $\beta \neq 0, 1/2$ the size of the chaotic zone on the (I, φ) cylinder is bounded from above (recall that we deal here with rescaled I variable; recall also that the chaotic zone corresponds to the level lines of J which intersect the separatrix set S). Moreover, it is now easy to give conditions under which the size of this zone is bounded away from zero. Indeed, inequalities (5.6) show that if

$$H \operatorname{sign} \beta + M > \frac{|\beta|}{2} \Lambda \max(0, \Lambda), \quad (5.7)$$

this zone is non-empty (recall that M is positive: $M = \varepsilon/\mu^4$).

6. The perturbed motion for regular β values

For sufficiently small μ , the slow-fast system (4.3) approximates the perturbed flow under the assumption that H , M and Λ , as well as the scaled variables I , p and q , stay bounded as $\mu \rightarrow 0$. In particular, as long as the chaotic zone has a finite extent in the rescaled I , the perturbed system has also a chaotic zone with similar properties that extends to $O(\mu^2)$ in I .

So far μ is an arbitrary scaling parameter, and $H = E/\mu^4$, $M = \varepsilon/\mu^4$, $\Lambda = \lambda/\mu^2$. For $\beta \neq 0, 1/2$ the scaled variables automatically remain bounded if H , M and Λ remain bounded: by proposition 5.4, even when the energy surfaces are unbounded in I , there are always horizontal curves of bounded rescaled $|I|$ values that are bounded away from the separatrix set; for sufficiently small μ these curves produce KAM tori that indeed bound the motion.

The following choice of μ guarantees that H , M and Λ remain bounded and that at least one of these parameters stays bounded away from zero:

$$\mu^4 = \varepsilon + |E| + \lambda^2. \quad (6.1)$$

If M stays bounded away from zero, the chaotic zone has a finite, bounded away from zero size in the rescaled coordinates (see (5.6)). Hence, by (4.1), the chaotic zone extent in the non-rescaled I is $O(\mu^2)$. As M is bounded away from zero, $\mu^2 = O(\sqrt{\varepsilon})$ and the extent of the chaotic zone is $O(\sqrt{\varepsilon})$ (here, by (6.1), the energy level and the tuning parameter satisfy $E, \lambda^2 = O(\varepsilon)$).

When $M \rightarrow +0$, formula (5.6) shows that the extent of the zone in the rescaled I is of order M if H remains bounded away from zero (so we have here $\mu^4 = O(E)$ and $|E| \gg \varepsilon$). In the original I variable we thus obtain that the chaotic zone at the energy level $H_{\text{par-res}} = E$ is of size $O(\mu^2 M) = O(\varepsilon/\mu^2) = O(\varepsilon/\sqrt{|E|})$. If both M and H tend to zero, Λ must stay bounded away from zero and be strictly negative (see (5.7)). In this case the chaotic zone extent in the rescaled I is of order $M/\sqrt{|H|}$ when $M = o(H)$ and of order \sqrt{M} otherwise. In the non-rescaled variable I , we find again that the size of the chaotic zone is of order $O(\varepsilon/\sqrt{|E|})$ if $E \gg \varepsilon$ and $O(\sqrt{\varepsilon})$ if $E = O(\varepsilon)$.

Rewriting condition (5.7) we thus arrive at the following main result:

Theorem 6.1. Consider a near-integrable Hamiltonian system having, in the integrable limit, a circle of fixed points which is normally parabolic and the corresponding normal form is given by (2.1). Let the normal form be non-degenerate, i.e. $\beta \neq 0, 1/2$. Then, the extent in I of the parabolic resonance chaotic zone (the union of all the J level sets that intersect the separatrix set), does not exceed $O(\sqrt{\varepsilon})$. Moreover, for any $K > 1$, there exists $Q > 0$ such that for the values of the energy satisfying

$$E \operatorname{sign} \beta + \varepsilon > K \frac{|\beta|}{2} \lambda \max(0, \lambda) \tag{6.2}$$

the I -extent of this zone on the level $H_{\text{par-res}} = E$ is bigger than $Q \frac{\varepsilon}{\sqrt{\varepsilon+|E|}}$.

Several properties of the chaotic zone may be now established:

Volume of the chaotic set. The chaotic zone was defined as a phase-space area in the rescaled (φ, I) plane. Each point (φ, I) in the slow-variables plane is associated (provided $J(\varphi, I) \neq 0$) with one or two fast closed orbits in the qp plane. So, a closed J level line in the slow plane corresponds to a torus in the phase space. The chaotic zone with the area of order 1 lifts to shells of tori (solid tori if $J = 0$ belongs to the chaotic zone) with the three-dimensional volume of order 1, and the union of these zones over the range of energies each having a chaotic zone with the area of order 1 has four-dimensional volume of order 1. Moreover, the extent of this chaotic set is of order one in each of the rescaled variables (q, p, φ, I) . By theorem 6.1, for $\lambda = O(\sqrt{\varepsilon})$, there exists such a range of energies (with $H_{\text{par-res}} = E = O(\varepsilon)$ so $\mu = O(\varepsilon^{1/4})$ by (6.1)). Thus, for this energy range, the extent of the chaotic set in the original (q, p, φ, I) directions is of order $(\varepsilon^{1/4}, \varepsilon^{1/2}, 1, \varepsilon^{1/2})$. Hence the four-dimensional volume of the chaotic set (on a range of energy surfaces of order ε) is

$$\text{Volume}_{\text{chaotic set}} = O(\varepsilon^{5/4}).$$

When $\beta > 1/2$, it is proportional to the volume of the energy surfaces near the parabolic resonant circle. For $\beta < 1/2$ the volume of the energy surface may be infinite, yet, the chaotic set volume is finite as long as $\beta \neq 0$.

Topology of the chaotic zone. The shape of the chaotic zone depends on the two parameters (β, λ) , on the energy value E and, in the (I, φ) plane, on the form of the perturbation term $V(\varphi)$. Qualitatively, it can be recovered from the EMBD skeletons and quantitatively it can be found from the plots of the J level sets on the EMBD as demonstrated in figures 7 and 8.

Parabolic resonance instability. For small E values that satisfy (6.2) the chaotic zone extends from negative to positive I values⁷. Then, the chaotic trajectories have a mixed behaviour, connecting the elliptic and the hyperbolic regime—the hallmark of the *parabolic resonance instability*. A necessary condition for such trajectories to exist, is that the intersection of the set $J_{\text{sep}}(H)$ of j values that satisfy (5.6) with the set $J_0(H)$ of j values that intersect the line $I = 0$ is non-empty. From (5.1) we find that

$$J(z, 0; \beta, \Lambda) = \sqrt{8} \int_{q_-}^{q_+} \sqrt{z - \frac{\beta}{2} \Lambda^2 - \frac{q^4}{4}} dq = 3.496... \left(z - \frac{\beta}{2} \Lambda^2 \right)^{3/4}$$

so, provided $H + M > \frac{\beta}{2} \Lambda^2$ we get that

$$J_0(H) = \left\{ j \mid \max \left(0, H - M - \frac{\beta}{2} \Lambda^2 \right) < \left(\frac{j}{3.496...} \right)^{4/3} < H + M - \frac{\beta}{2} \Lambda^2 \right\}, \tag{6.3}$$

⁷ In contrast, when $|E|$ is sufficiently large, the chaotic zone has a rectangular shape that is composed of horizontal j level lines that are limited to positive I values. Then, the usual homoclinic chaos emerges.

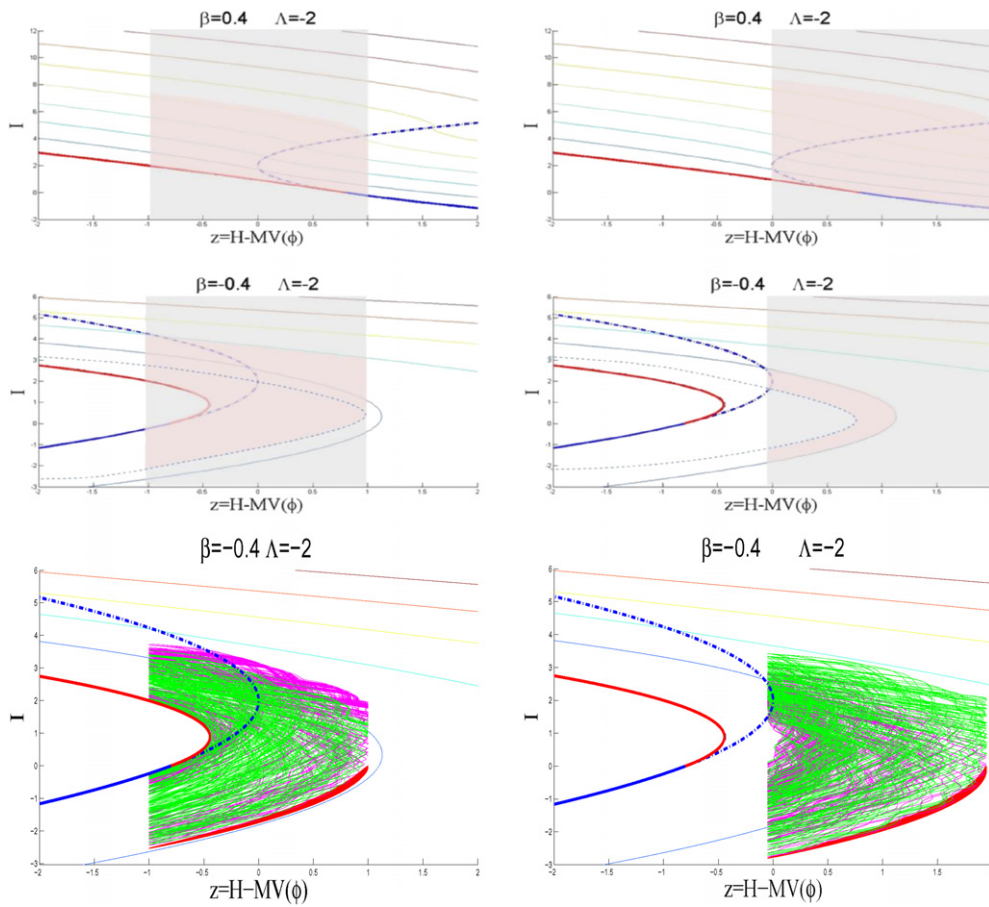


Figure 7. Analytic prediction and numerical realizations of the chaotic zone shape, location and size in the modified EMBD for different energies (right $H = 0$, left $H = 0.95$) and parameter values ($\Lambda = -2$, $M = 1$, $\beta = 0.4$ (a)–(b), or -0.4 (c)–(f)). Panels (a)–(d): Coloured curves—the J level sets as in figure 6, the light grey region— D_H ; the darker pink region—chaotic zone. Panels (e)–(f)—numerical realizations (at $\varepsilon = 0.05$) corresponding to panels (c)–(d). The predicted zone and the numerical realizations agree well at $H = 0$, while at $H = 0.95$ the chaotic set is larger than predicted due to finite ε effects (see figure 8).

while $j \in J_{\text{sep}}(H)$ when H, M, Λ satisfy (5.7), and (see (5.6))

$$H - M - \frac{\beta}{2} \Lambda^2 < \frac{\beta}{2} \left(\frac{j}{1.333\dots} \right)^{4/3} + \beta \Lambda \left(\frac{j}{1.333\dots} \right)^{2/3} < H + M - \frac{\beta}{2} \Lambda^2.$$

For example, at $\Lambda = 0$ we conclude that $J_0(H) \cap J_{\text{sep}}(H) \neq \emptyset$ when

$$-1 < \frac{H}{M} < \max \left(1, \frac{1 + 1.8079\dots\beta}{|1 - 1.8079\dots\beta|} \right) \tag{6.4}$$

so the parabolic resonance instability appears at energies E of order $O(\varepsilon)$. When $\beta \approx 0.5531$ the denominator on the right hand side vanishes. Numerically, we find that for this β value the parabolic resonance instability is indeed seen for rather large energies ($\frac{H}{M} \lesssim 10$). For larger H values, the level sets that belong to $J_{\text{sep}}(H)$ are split into two parts by the boundaries of D_h , so the segments that cross the separatrix and the segments that cross the $I = 0$ line are

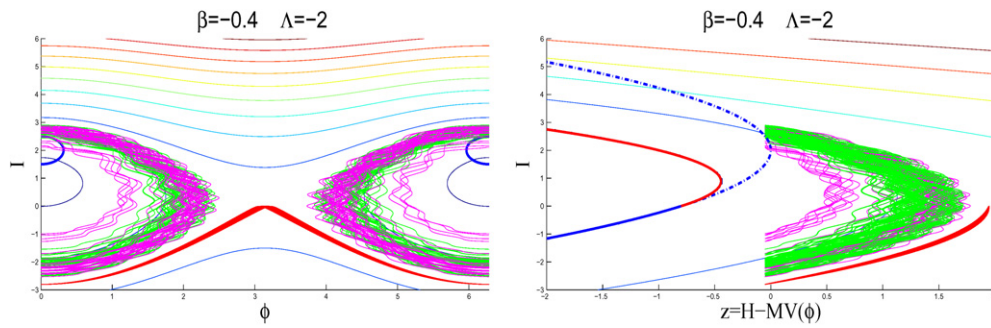


Figure 8. The chaotic zone in the slow-variable space (left). The J level curves are found by reflection of the J -segments in the modified EMBD plot (right) that are restricted to D_H . The topology, location and size of the chaotic zone in the slow-variable space may be thus determined from the modified EMBD plots. Here, at $\varepsilon = 0.01$ the shape and extent of the chaotic region are closer to the prediction (compare with figures 7(d) and (f), where, at $\varepsilon = 0.05$, the chaotic zone merges with the region associated with the slow separatrices splitting).

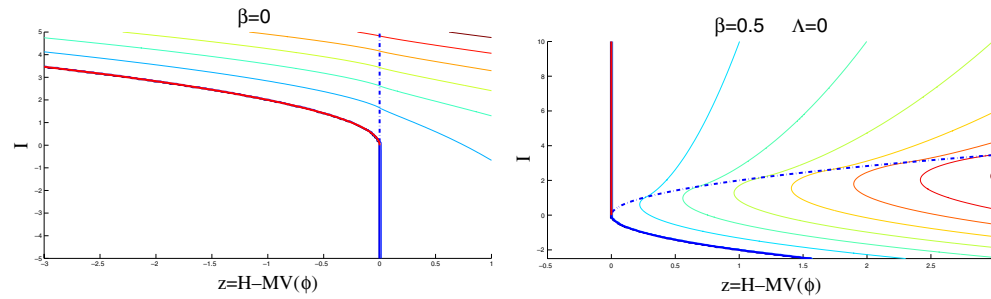


Figure 9. The J level lines for the singular β values.

disconnected, and the parabolic resonance instability is arrested. Summarizing, for all non-degenerate β 's, at $\lambda = 0$, there is an $O(\varepsilon)$ range of energies for which the parabolic resonance instability is observable.

7. Degenerate instabilities—the singular β values

The structure of the chaotic zone changes drastically as β passes through the singular values $\beta = 1/2$ and $\beta = 0$, the two degenerate cases. To analyse these, we first study the EMBD structure and the resulting dynamics of the limit system (equation (4.3) without the $O(\mu)$ terms), where we show that some of the level sets of J are vertical (figure 9) and thus that the resulting motion is unbounded in I . We then examine, under some simplifying assumptions on the form of the perturbation, the effect of the higher order terms on the extent of the level sets and the extent of the chaotic zone.

7.1. The parabolic resonance V-instability $\beta = 1/2, \Lambda = 0$

7.1.1. The limit system. Here, the semi-parabola L_{\pm} in the EMBD degenerates to a ray with a $\Lambda/2$ slope: $L_{\pm, \beta=1/2} : z = \frac{\Lambda}{2} + \frac{\Lambda^2}{4}, I \geq 0$. At $\Lambda = 0$ this ray is vertical, the corresponding family of circles is $\{q = \pm\sqrt{I}, p = 0\}$ and the phase velocity on the circles vanishes. The

ray L_{\pm} thus represents two semi-infinite cylinders that meet at $I = 0$ (the vertex of a V shape in the (q, p, I) space). At $\mu = 0$, these are cylinders of fixed points, the iso-energetic non-degeneracy condition of the KAM theory fails everywhere on this surface and hence, under perturbation, order one instabilities are possible.

When $\mu \neq 0$, the adiabatic theory for the limit system ($\mu \neq 0$ yet the $O(\mu)$ terms dropped) may be utilized as before. The ray L_{\pm} belongs to the $J = 0$ level set and is fully contained in the energy strips D_H for all $H \in (-M, M)$. The structure of nearby level sets at $I > 0$ may be extracted by setting $\beta = 1/2, \Lambda = 0$ in (5.4) to obtain

$$J(z, I; 1/2, 0) = \sqrt{8}I^{3/2}K\left(\frac{z}{I^2} - \frac{1}{4}, +\right) = \sqrt{8}\frac{z}{I^{1/2}}K'\left(-\frac{1}{4}, +\right) + O\left(\frac{z^2}{I^{5/2}}\right).$$

This shows that the level sets in the large I and small j limit are given by $z = \frac{j\sqrt{I}}{\sqrt{8K'(-\frac{1}{4}, +)}} + O(I^{-1})$, and these intersect the line $z = H + M$ at

$$I_{\max}(j) = \frac{8}{j^2} \left((H + M)K'\left(-\frac{1}{4}, +\right) \right)^2 + O(j^2).$$

Moreover, it follows from (5.6) that for $|H| < M$

$$J_{\text{sep}}(H)_{\beta=1/2, \Lambda=0} = [0, 8(H + M)^{3/4}K(0, +)],$$

so the chaotic set for these energy levels extends to infinity, connecting initial conditions with negative actions to unbounded heights. Trajectories that start at arbitrary small I values above the separatrix set climb up along one edge of the V and follow a $J = j$ level set till this level set crosses the line $z = H + M$ at $I \propto 1/j^2$. Then the trajectory turns back down till it reaches the separatrix set, changes its j level, possibly goes down along a new j level line (the motion downward is bounded), up again, crosses the separatrix set one more time (changing j again to obtain j_{new}) and possibly climbs up again to a possibly different edge of the V -shape and to the new limiting I value which is proportional to $1/j_{\text{new}}^2$. Notably, symmetry is important—it may cause two consecutive changes in j to almost cancel out and produce stable recurrent motion, see [27] and the discussion in section 8.2.

The effect of detuning ($\Lambda = o(1), \beta = \frac{1}{2} + \tilde{\beta}, \tilde{\beta} = o(1)$) is analysed next. The $J = 0$ level line intersects the boundary of the energy surface H at (see (5.1)):

$$H \pm M = \frac{\tilde{\beta}}{2}(I + \Lambda)^2 + \frac{I\Lambda}{2} + \frac{\Lambda^2}{4}.$$

Thus, since $|H| < M$ (so $\text{sign}(H \pm M) = \pm 1$), we find

$$I_{\max}(\Lambda) = \frac{2}{\Lambda} \left(H + M \text{sign } \Lambda - \frac{\Lambda^2}{4} \right) \quad \text{for } \tilde{\beta} = 0$$

$$I_{\max}(\tilde{\beta}, \Lambda) = -\Lambda \left(1 + \frac{1}{2\tilde{\beta}} \right) + \frac{|\Lambda|^2}{|\tilde{\beta}|} \sqrt{1 + 2\tilde{\beta} + \frac{8}{\Lambda^2}(\tilde{\beta}H + |\tilde{\beta}|M)} \quad \text{for } \tilde{\beta}, \Lambda \neq 0$$

$$\approx \begin{cases} \frac{2}{\Lambda} \left(H + M \text{sign } \Lambda - \frac{\Lambda^2}{4} \right) & \tilde{\beta} = o(\Lambda^2), \\ O(1/\Lambda) & \tilde{\beta} \sim \Lambda^2, \\ \sqrt{\frac{2}{\tilde{\beta}}} \sqrt{H + M} & \Lambda^2 = o(\tilde{\beta}). \end{cases} \tag{7.1}$$

Summarizing, in the limit system, at $\beta = \frac{1}{2} + \tilde{\beta}, \tilde{\beta} = o(1), \Lambda = o(1)$, the extent of the instability zone for $|H| < M$ is at least $O\left(\frac{1}{|\Lambda| + \sqrt{|\tilde{\beta}|}}\right)$. If both $\tilde{\beta}$ and Λ are positive, the upper

bound on the extent in I of the energy surface, hence—of the chaotic zone, is also of the same order. The implications of other sign combinations of $\tilde{\beta}$ and Λ need to be further studied: the $J = 0$ level line may be directed to the left, the energy surfaces with small positive E are unbounded, and then I_{\max} provides only a lower bound to the extent of the chaotic set.

7.1.2. The perturbed dynamics. The terms of the Hamiltonian (2.1) that are neglected in the limit system, $G_{\text{pert}}(q, p, I, \varphi) = \varepsilon V_{\text{pert}}(q, p, I, \varphi) + F(p, q, I) - \varepsilon V(\varphi)$, remain small in the rescaled system if the trajectories remain in some small neighbourhood of the parabolic resonant circle (recall that $G(q, p, I, \varphi) := \frac{1}{\mu^5} G_{\text{pert}}(\mu q, \mu^2 p, \mu^2 I, \varphi)$ appears in the rescaled Hamiltonian (4.2)). However, as we have seen, in the degenerate cases the limit system may have orbits for which (the rescaled) I grows without bounds. Near such orbits the G -terms can no longer be neglected. We do not aim in this paper to build a full theory of what may happens. Instead, we consider two basic cases.

Flat case. If $G(q, p, I, \varphi)$ is such that it and its derivatives remain bounded for arbitrarily large real arguments corresponding to the stable equilibria $\{q = \pm\sqrt{I}, p = 0\}$ of the fast subsystem, then the limit system provides the leading order behaviour of the perturbed dynamics (as we have seen, the maximal growth in I occurs near the surface corresponding to these equilibria). We thus conclude that in this case the extent of the chaotic zone in the original coordinates is at least of order $O(\frac{\varepsilon}{|\lambda| + \sqrt{\varepsilon|\tilde{\beta}|}})$, thus, for $\sqrt{\varepsilon|\tilde{\beta}|} + |\lambda| = O(\varepsilon)$, the motion in I is at least of order one for a range of energies satisfying $|E| < \varepsilon$.

A common example for this case is when the perturbation depends only on φ : $V_{\text{pert}}(q, p, I, \varphi) = V(\varphi)$ and the higher order terms vanish $F(q, p, I) \equiv 0$. Then $G \equiv 0$ and the flatness conditions are trivially satisfied. Surprisingly, this particularly degenerate situation does appear in several applications (see [20, 27, 33, 35] and section 8).

Higher power nearly flat case. If $G_{\text{pert}}(q, p, I, \varphi) = aI^{2+n}$ then the tori $\{q = \pm\sqrt{I}, p = 0\}$ filled by normally elliptic invariant circles remain invariant, and, at $\tilde{\beta} = \lambda = 0$, the system on the torus has the energy:

$$H_{\text{par-res}}(I, \varphi) = \varepsilon V(\varphi) + aI^{2+n}.$$

Thus, this torus intersects the energy surface $H_{\text{par-res}}(I, \varphi) = \varepsilon H$ at the circle $I_{L\pm}(\varphi; H) = \varepsilon^{\frac{1}{n+2}} (\frac{H-V(\varphi)}{a})^{\frac{1}{n+2}}$. Note that near this circle the fast-slow structure is preserved; The normal frequency near $(q, p) = (\pm\sqrt{I}, 0)$ is of order \sqrt{I} , namely of order $O(\varepsilon^{\frac{1}{2n+4}})$ whereas the frequency in φ is of order I^{n+1} , namely of order $O(\varepsilon^{\frac{n+1}{n+2}})$. Indeed, we may utilize the analysis of section 4 by replacing the assignment (6.1) for μ by $\mu = \varepsilon^{\frac{1}{2n+4}}$. Then, the rescaled I is finite for the values of the non-rescaled I of order $O(\varepsilon^{\frac{1}{n+2}})$ and we thus conclude that the perturbed motion follows the adiabatic invariant level lines up to this order of I values. Here, a delicate issue arises; the leading order approximation of the adiabatic invariant is given by (5.1). The correction terms have a contribution from both the higher order terms $G(I, \varphi)$ and from the second order averaging, thus finding this correction to the J level lines is not immediate. Nonetheless, the above calculation of the energy on the circles belonging to the invariant plane $(q, p) = (\pm\sqrt{I}, 0)$ allows us to compute the $J = 0$ level line to all orders, and thus conclude that for energy levels with $|H| < M$ the chaotic zone extent is bounded from below by $O(\varepsilon^{\frac{1}{n+2}})$. In the multi-dimensional setting the higher power nearly flat parabolic resonances is a persistent phenomenon [22].

We believe that for more general unfolding the behaviour is similar to that described above: while the torus of normally elliptic invariant circles is no longer preserved, it is replaced by

a torus which is nearly invariant (up to corrections exponentially small in ε) [15]. Therefore, the $O(\varepsilon^{\frac{1}{n+2}})$ excursions in I along the edges of the V shape remain a typical phenomenon.

7.2. The parabolic resonance well-to-chain instability $\beta = 0$

7.2.1. The limit system. The parabola L_0 of the EMBD degenerates here to a vertical line which is contained in all energy surfaces with $H \in (-M, M)$. Two different mechanisms for unbounded motion are thus created: a transition chain in the positive I direction and a deep well in the negative I direction.

Transition chain. For $\mu = 0$, the ray L_0^+ corresponds to a torus of fixed points each having a pair of zero eigenvalues and a pair of real non-zero eigenvalues (of order $O(\sqrt{I})$). This normally hyperbolic manifold has a homoclinic connecting manifold. For non-zero μ , the normally hyperbolic manifold persists (it is in fact unchanged since $G \equiv 0$ on it). The homoclinic connecting manifold splits and transition chains to arbitrarily large I values may emerge (techniques for studying *a priori* unstable systems may be employed to prove this, see [7, 8, 41, 42] and references therein). The passage to this transition-chain region is well described by the rescaled limit system: for sufficiently large I of the rescaled system ($I \gg M/K(0, +)$) the level sets become horizontal and intersect L_0^+ transversely (see the proof of proposition 5.3 and note that expansion (5.5) for the upper level curves $I_+(z)$ is regular at $\beta = 0$).

When the orbits in the transition chain approach small I values, substantial periods are spent along parts of the level lines of J that are bounded away from the separatrix set and involve both elliptic and hyperbolic behaviour. Indeed, since the J level sets at $\beta = 0$ are monotonically decreasing in z (differentiate (5.1)), the level line with $j_s = 3.496\dots(H+M)^{3/4}$ (see (6.3)) separates between the level sets having only hyperbolic behaviour (with $j > j_s$) and those having elliptic-to-hyperbolic behaviour (with $j < j_s$). The corresponding critical I value on \mathcal{M} is thus $I_s = (\frac{j_s}{\sqrt{8K(0,+)}})^{2/3} = 1.901\dots(H+M)^{1/2}$.

Deep well. The vertical ray L_0^- corresponds here to the $J = 0$ level set. As in the flat V case, the nearby small j level curves are unbounded in the negative direction, creating an infinitely deep well. More precisely, the level sets structure at large ($-I$) and small j limit may be extracted by setting $\beta = 0$ in (5.4) and expanding in $z/(-I)^2$ to obtain $z = \frac{j\sqrt{-I}}{\sqrt{8K'(0,-)}} + O(I^{-1})$, and these intersect the line $z = H + M$ at $I_{\min}(j) = -\frac{8}{j^2}((H+M)K'(0,-))^2 + O(j^2)$.

Summarizing, trajectories of the perturbed limit system can have unbounded motion in both the positive and negative I directions. In the negative I direction trajectories experience long excursions by which I decreases at its maximal possible rate (with $\dot{I} = O(\varepsilon)$) and the motion in the (q, p) plane corresponds to fast oscillations. This deep dive into the well stops and reverses to a climb when the j level set intersects the line $z = H + M$ (the smaller is the j , the deeper is the dive). After the trajectory had climbed up, along a level set of J , to the region $I > 0$, it intersects the separatrix set—the positive I axis—and then the j value changes. The changes in j near $I = 0$ depend sensitively on the crossing phase, and thus, the trajectory may either ‘diffuse’ up by a series of jumps in j or jump back down to the well again, where the new value of j determines the depth of the dive.

If Λ and β are small, the above scenario is still relevant: the manifold of fixed points deforms to the parabola $z = \beta(I + \Lambda)^2$ and thus intersects the energy surface boundaries at the large I values $I_{\pm} = \pm\sqrt{\frac{H+M\text{sign}\beta}{\beta}} - \Lambda$. For positive β , I_- provides a bound to the energy

surface extent in the negative I direction: $O(\sqrt{\frac{H+M\text{sign}\beta}{\beta}})$. For negative β , this value is only a lower bound. The upper value I_+ provides an upper bound to the extent of the transition chain on the energy surfaces with $|H| < M$.

7.2.2. *The perturbed dynamics.* As in the V instability case, there are two main cases of the perturbation term:

Flat case. If $G(q, p, I, \varphi)$ and its derivatives remain bounded for arbitrarily large real arguments, then the limit system provides the leading order behaviour of the perturbed dynamics. Thus, the extent of the chaotic zone in the original coordinates is at least of order $O(\sqrt{\frac{\varepsilon}{|\beta|}})$ for energies satisfying $|E| < \varepsilon$.

Higher power nearly flat case. If $G_{\text{pert}}(q, p, I, \varphi) = aI^{2+n}$ then the torus $q = 0, p = 0$ of unperturbed invariant circles remains invariant, and at $\beta = \lambda = 0$ the energy of the system on the torus is $H_{\text{par-res}}(I, \varphi) = \varepsilon V(\varphi) + aI^{2+n}$. Thus, this torus intersects the energy surface $H_{\text{par-res}}(I, \varphi) = \varepsilon H$ at the circle (s): $(I_0(\varphi; H))^{n+2} = \varepsilon(\frac{H-V(\varphi)}{a})$. Here different cases arise when a is positive/negative and when n is even/odd, yet the principle behaviour is clear: as in the $\beta = 1/2$ case, we may utilize the analysis of section 4 by replacing the assignment (6.1) for μ by $\mu = \varepsilon^{\frac{1}{2n+4}}$. Then, the rescaled I is finite for $I = O(\varepsilon^{\frac{1}{n+2}})$ and we thus conclude that the perturbed motion follows adiabatic invariant level lines up to these I values, and the conclusions regarding the limit system all apply up to these larger I values.

8. Three applications

8.1. The motion of weather balloons

At high-altitude (10–15 km above sea level) the motion of inertial particles on a rotating sphere adequately mimics the weather balloons motion [31]. Non-dimensional Lagrangian momentum equations for the eastward and northward velocity components (u, v) and the rate of change of the longitude and latitude coordinates (θ, ϕ) in the presence of a stationary zonally symmetric pressure field $B(\phi)$ and a zonally travelling pressure wave with small amplitude $A(\phi)$ (both assumed to be even in ϕ) are given by

$$\begin{aligned} \frac{d\theta}{dt} &= \frac{u}{\cos\phi}, & \frac{du}{dt} &= v \sin\phi \left(1 + \frac{u}{\cos\phi}\right) - k\varepsilon \frac{A(\phi)}{\cos\phi} \cos(k\theta - \sigma t) \\ \frac{d\phi}{dt} &= v, & \frac{dv}{dt} &= -u \sin\phi \left(1 + \frac{u}{\cos\phi}\right) - \varepsilon A'(\phi) \sin(k\theta - \sigma t) - B'(\phi) \end{aligned} \tag{8.1}$$

This model was introduced with $A(\phi) = B(\phi) = 0$ and numerically studied in [31]. It was analysed in the perturbed case $A(\phi) \neq 0, B(\phi) = 0$ in [34]. In [35] it was realized that $B(\phi) = 0$ corresponds to a flat parabolic resonance instability, see below.

When $A(\phi) = 0$ the motion is integrable: system (8.1) has two integrals, corresponding to (twice) the angular momentum I and the energy E ,

$$I = \cos\phi(\cos\phi + 2u), \quad E = \frac{1}{2}(u^2 + v^2) + B(\phi).$$

Using I as a variable, for finite wave-length perturbations ($k \neq 0$, so set $\varphi = \frac{\theta}{2} - \frac{\sigma}{2k}t$), the Hamiltonian becomes

$$H(\phi, v, \varphi, I) = \frac{v^2}{2} + \frac{1}{8} \left(\frac{I}{\cos\phi} - \cos\phi \right)^2 - \frac{\sigma}{2k} I + B(\phi) + \varepsilon A(\phi) \sin(2k\varphi). \tag{8.2}$$

At $B(\phi) \equiv 0$, for the unperturbed problem, in the (ϕ, v) plane, the origin is hyperbolic at $I \in (-1, 1)$, and has two symmetrical homoclinic orbits. At $I = \pm 1$ the origin becomes parabolic. Thus, we have a parabolic resonance. One may check that at $I = 1$ the normal form parameters are

$$\beta = \frac{1}{2}, \quad \Lambda = 4\sigma k, \quad \epsilon = 8k^4 A(0).$$

So, we obtain that for $B(\phi) = 0$ and for standing waves perturbations ($\sigma = 0$) the normal form parameters correspond to the V -instability from section 7.1. The stable equilibria of the fast (v, ϕ) subsystem are given by $I = \cos^2 \phi$, and we see that when the system is restricted to these (v, ϕ) -values, the energy constraint (8.2) does not provide any bound on I at $\sigma = 0$, $B \equiv 0$. Therefore, we have a flat V -instability in this case, which means (see section 7.1.2) that large deviations in I are possible for arbitrarily small ϵ .

Thus, if no stationary pressure wave is included, unbounded motion may appear even for particles that are released near the equator ($\phi = 0$), have small initial velocities, and are driven by small fluctuations of the pressure field—roughly the wind velocity. This surprising finding may explain some strange balloons trajectories that were observed in field experiments in which the weather balloons were released near the equator and were tracked for a month. Most of the balloons remain around the equator region: most of the initial conditions do not have the correct phase to enter, during the limited experimental observation time, a small neighbourhood of the $J = 0$ level line (which corresponds to the stable equilibria of the fast subsystem and is the only root along which long excursions in I are possible at $\beta = 1/2$). The exceptional initial conditions (two balloons out of 512) should have corresponded to the correct phase, so $J \approx 0$, and thus the balloons undergo excursions extending to the polar regions. Notably, counter to usual intuition, this unbounded motion in the model occurs even though there are no significant northern/southern winds that may carry the balloons to the poles on a time scale of one month. See [35] for further details and references.

8.2. The motion of a charged particle in the Earth magnetotail

The following non-dimensional Hamiltonian describes the charged particle motion (see [27] for references, motivation, derivation and analysis):

$$H = \frac{1}{2}(y^2 + p^2 + (\eta - (\epsilon\bar{x} - \frac{1}{2}q^2))^2),$$

where (q, p) are fast and $(x = \epsilon\bar{x}, y)$ are slow. Setting $I = 4(\epsilon\bar{x} - \eta)$, $p_{\text{new}} = 2\sqrt{2}p$, $q_{\text{new}} = \sqrt{2}q$, we obtain

$$H = \frac{1}{8}\hat{H} = \frac{1}{8}(\frac{1}{2}p^2 - \frac{1}{2}Iq^2 + \frac{1}{4}q^4 + \frac{1}{4}I^2 + 4y^2).$$

Namely, $8\hat{H}$ is exactly the Hamiltonian (4.2) in the degenerate flat V -case $\beta = 1/2$, $\Lambda = 0$ with the perturbation term $V(y) = 4y^2$. The perturbation here is degenerate (independent of (q, p, I)) and thus does not lift the flat V -degeneracy (here the y variable is non-cyclic—yet, the energy constraint provides a bound on y). Interestingly, for any \hat{H} the energy surface $D_{\hat{H}}$ in the (z, I) space, where $z = \hat{H} - 4y^2$, appears here as the slab $D \cap \{z \leq \hat{H}\}$, see figure 10. From these plots, the dependence of the chaotic zone topology on the energy may be found. For example, we see that already at $\hat{H} = 1$ some level sets do not cross the separatrices, so a small domain of stability persists. A slightly modified model for the Earth magnetotail—for example an asymmetric profile for the magnetic field—would have essentially different features as it lifts the degeneracy which allows unbounded motion. Finally, if the variations in the x -velocity term, y , are *a priori* bounded, then the energy surfaces appear as strips (as in the previous sections) and so for sufficiently large energies the degenerate behaviour near

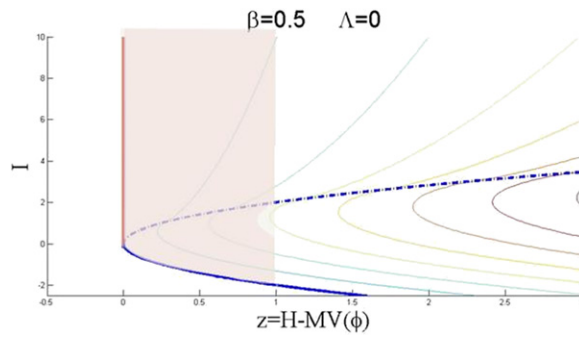


Figure 10. Energy surface $\hat{H} = 1$ for the charged particle in the Earth magnetotail: the J level lines are exactly as in figure 9.

the origin will not be included in $D_{\hat{H}}$. In such a case, for large \hat{H} , only finite instabilities are possible.

Combing this new framework for analysing this system with the previous extensive analysis of this model may be of value in studying the qualitative differences between the induced motion for various models of the magnetotail.

8.3. Truncated forced nonlinear Schrodinger model

The forced one-dimensional periodic nonlinear Schrodinger equation is a paradigm model for the appearance of non-integrability in PDEs. A two mode Galerkin truncation of this model turned out to be useful in gaining insight to the dynamics of the PDE solutions [2, 18, 36, 38], and is given by the following two-degrees-of-freedom near-integrable Hamiltonian system:

$$H(c, c^*, b, b^*; \varepsilon) = H_0(c, c^*, b, b^*) + \varepsilon H_1(c, c^*, b, b^*),$$

with the Poisson brackets $\{\cdot, \cdot\} = -2i(\frac{\partial}{\partial c}, \frac{\partial}{\partial c^*}) - 2i(\frac{\partial}{\partial b}, \frac{\partial}{\partial b^*})$, where

$$\begin{aligned} H_0 &= \frac{1}{8}|c|^4 + \frac{1}{2}|bc|^2 + \frac{3}{16}|b|^4 - \frac{1}{2}(\Omega^2 + k^2)|b|^2 - \frac{\Omega^2}{2}|c|^2 + \frac{1}{4}Re(bc^*)^2, \\ H_1 &= \frac{i}{\sqrt{2}}(c - c^*). \end{aligned} \tag{8.3}$$

At $\varepsilon = 0$, these equations are integrable: the additional integral is $I = \frac{1}{2}(|c|^2 + |b|^2)$. The equations possess families of periodic solutions of the form $c = |c| \exp(i\omega t + i\theta)$, $b = |b| \exp(i\omega t + i\theta)$. One of these families, the plane-wave solutions (the circles with $b = 0$), undergoes a bifurcation from being elliptic to hyperbolic. The parabolic resonance appears when the plane-wave circle at which this bifurcation occurs has the same frequency as the forcing [36]. The parabolic resonance normal form is found by a series of transformations. First, we transform to the generalized action angle coordinates (x, y, I, γ) [18]:

$$c = |c| \exp(i\gamma), \quad b = (x + iy) \exp(i\gamma), \quad I = \frac{1}{2}(|c|^2 + x^2 + y^2),$$

so $(I, \gamma) \in (R^+ \times T)$, $(x, y) \in B_I = \{(x, y) | x^2 + y^2 < 2I\}$, and the Hamiltonian (8.3) becomes

$$\begin{aligned} H_0(x, y, I) &= \frac{1}{2}I^2 - \Omega^2 I + (I - k^2/2)x^2 - \frac{7}{16}x^4 - \frac{3}{8}x^2 y^2 + \frac{1}{16}y^4 - \frac{1}{2}k^2 y^2, \\ H_1(x, y, I, \gamma) &= \sqrt{2} \sin \gamma \sqrt{2I - x^2 - y^2}. \end{aligned}$$

The plane-wave branch, at which $b = 0$ (so $x = y = 0$), is defined by $|c| = \sqrt{2I}$. The corresponding frequency is $\omega^{\text{pw}} = I - \Omega^2$, and resonance happens at $I_r^{\text{pw}} = \Omega^2$. The family is stable for $I < I_p^{\text{pw}} := \frac{1}{2}k^2$ and unstable for $I > I_p^{\text{pw}}$. Hence, we have a parabolic resonance when $I_r^{\text{pw}} = I_p^{\text{pw}}$, i.e. at $\Omega_{\text{pr-pw}} = \frac{1}{\sqrt{2}}k$. Shifting the origin to the resonant circle $\tilde{I} = I - \frac{1}{2}k^2$, denoting $\lambda = \frac{1}{2}k^2 - \Omega^2$, and then making the rescaling $(x, y, \tilde{I}, \gamma, t, H, \lambda)_{\text{nls}} \rightarrow (ax, by, abI, \gamma, -t/k^2b^2, -k^2b^2H, ab\lambda)_s$ with $a = \frac{\sqrt{7}}{4}k$, $b = 2(\frac{\sqrt{7}}{4})^3k$ brings the Hamiltonian to the parabolic resonance normal form:

$$H_0(x, y, I) = \frac{1}{2}y^2 - \frac{1}{2}Ix^2 + \frac{1}{4}x^4 - \frac{7}{32}(I + \lambda)^2 + \frac{21}{128}x^2y^2 - \frac{7^3}{47}y^4 + \frac{512}{7^3} \frac{\Omega^4}{k^4},$$

$$H_1(x, y, I, \gamma) = -\frac{1024\sqrt{2}}{7^3} \frac{1}{k^3} \sin \gamma \sqrt{1 + \frac{7^2}{4^3}I - \frac{7}{16}x^2 - \frac{7^3}{4^5}y^2}.$$

The final rescaling to the parabolic resonance region $(x, y, I, \gamma, t, H, \lambda)_s \rightarrow (\mu x, \mu^2 y, \mu^2 I, \varphi - \pi/2, t/\mu, \mu^4 H, \mu^2 \Lambda)_{nf}$ brings the Hamiltonian near the resonant plane wave to the rescaled normal form (4.2), where $V(\varphi) = \cos \varphi$, and the dependence of the normal form parameters (Λ, β, M, H) on the NLS parameters $(k, \Omega, \varepsilon_{\text{nls}}, H_{\text{nls}})$ is given by

$$\Lambda = \frac{1}{\mu^2} \frac{128}{49} \left(\frac{1}{2} - \frac{\Omega^2}{k^2} \right), \quad \beta = -\frac{7}{16}, \quad M = \frac{\sqrt{2}4^5}{7^3} \frac{1}{k^3} \frac{\varepsilon_{\text{nls}}}{\mu^4},$$

$$H = -\frac{1}{\mu^4} \frac{1}{k^4} \frac{4^5}{7^3} \left(H_{\text{nls}} + \frac{1}{2}\Omega^4 \right).$$

The parameter β , that enters the degeneracy condition, is fixed and negative and thus the parabolic resonance of the forced NLS is always regular. The EMBDs near the resonant circle are the two most left diagrams of figure 1, and indeed, comparing them with the diagrams of [36] shows exactly these two cases as Ω^2 is varied. Note that $\frac{H}{M} = -\frac{1}{k} \frac{H_{\text{nls}} + \frac{1}{2}\Omega^4}{\sqrt{2\varepsilon_{\text{nls}}}}$. So, by (6.4), the range of energies at which the parabolic resonance instability is observable increases linearly with k . At $H, M = O(1)$, the effective perturbation parameter is $\mu \propto (\varepsilon_{\text{nls}}/k^3)^{1/4}$, namely, the validity of our adiabatic-chaos description depends on this ratio. Notably, it was recently demonstrated numerically that when μ is sufficiently small solutions of the full PDE also preserve the adiabatic invariant of this truncated normal form. Hence, for sufficiently small ε , the normal form provides *a priori* estimates to the extent of the instability in the PDE [39].

9. Summary and discussion

The perturbed behaviour near a symmetric (generating a ‘figure-eight’) parabolic resonant circle can be of six different regular types, and there are two degenerate border cases. In all cases, for an $O(\varepsilon)$ range of energies, the instability is observable: there is a set, with a phase-space volume which is polynomial in ε , at which trajectories exhibit adiabatic-type chaos.

The scaling of the *volume of the chaotic set* with ε emerged here as a measure that distinguishes between the behaviour near the three different resonant circles that arise in one parameter families of two-degrees-of-freedom near-integrable systems: the hyperbolic, elliptic and parabolic resonant circles. While all three circles have identical resonant dynamics in the ‘almost-invariant’ plane ($q = p = 0$), their behaviour in the normal direction is distinct. In the elliptic case, under small perturbations, most of the perturbed phase space is foliated by KAM tori, and only an exponentially narrow region around the (I, φ) separatrices is excluded. Thus, in this elliptic resonance case, while the extent in I of the resonant orbits is of order $\sqrt{\varepsilon}$,

the volume of the chaotic set is *exponentially small*. In the hyperbolic resonance case we are not aware of any estimates of this volume—previous studies focused on finding multi-pulse homoclinic orbits and did not include information on the bulk properties of the chaotic zone. It is an important question that needs to be addressed in a future work. Note that by KAM theory this volume is certainly not larger than $O(\sqrt{\varepsilon})$. For the non-degenerate parabolic resonance case we found that the chaotic zone volume is of order $\varepsilon^{5/4}$. We thus propose that the parabolic resonance provides the dramatic transition from an exponentially small, ‘invisible’ chaos in the elliptic resonance regime to the clearly observable homoclinic resonance regime.

Methodologically, two main steps were taken to analyse the dynamics:

- (1) Rescaling, with a parameter μ that depends on the energy level, the perturbation size and the bifurcation parameter, brought the system to a slow-fast form. Then the adiabatic-chaos framework was utilized to analyse the perturbed flow and identify the chaotic zone.
- (2) Projecting of the adiabatic level sets and the separatrix set to the modified energy–momentum diagram (the $(z = \frac{E-\varepsilon V(\varphi)}{\mu^4}, \frac{I}{\mu^2})$ plane) provided qualitative and quantitative predictions for the extent and topology of the chaotic zone simultaneously for all energy levels.

These methods may be utilized to study other parabolic resonant bifurcations: other symmetric cases (hyperbolic pitchfork and a symmetric pair of simultaneous parabolic resonances), the influence of slight asymmetry on the symmetric configurations, as well as the generic non-symmetric parabolic resonant bifurcation in both the compact and non-compact level-sets cases.

Applying other methods, such as the adiabatic separatrix crossing map [9, 10, 28] may reveal additional properties of the parabolic resonance trajectories; First, it may be used to study what is the measure of the stability islands inside the chaotic set for general parameter values and perturbations (as in [27] for the specific case $\beta = 1/2, V(\varphi) = \varphi^2$). It can also be utilized to study the topology and knot-property of the islands, thus establishing lower bounds on the topological entropy of the perturbed problem. Moreover, this map may be used for proving accessibility-type results.

Finally, we remark that parabolic resonances naturally arise in multi-dimensional Hamiltonians, and thus one may generalize the current analysis to the higher-dimensional settings (see also [22, 37]):

$$H_{\text{par-res}} = \frac{p^2}{2} - I \frac{q^2}{2} + \frac{q^4}{4} + \beta(J) \frac{(\Lambda(J) + I)^2}{2} + \langle \omega, J \rangle + \frac{1}{2} J^T B J + \varepsilon V_{\text{pert}}(q, p, I, \varphi, J, \theta; \varepsilon),$$

$$\beta(0) = \beta_0, \quad \Lambda(0) = 0, \quad (q, p, I, \varphi, J, \theta) \in \mathbb{R}^3 \times \mathbb{T} \times \mathbb{R}^m \times \mathbb{T}^m.$$

One may hope that for non-degenerate values of β_0 ($\beta_0 \neq 0, \frac{1}{2}$) and Diophantine ω the two-degrees-of-freedom description may be still valid in the limit of sufficiently small ε . In this higher-dimensional setting degenerate cases are expected to appear persistently and should be studied.

Acknowledgments

The authors thank H Hansmann, A Neishtadt and E Shlizerman for important comments and discussions. They acknowledge the support of the Israel Science Foundation (Grant 273/07), Minerva foundation, Russian-Israeli joint grant (MNTI-RFBR No 06-01-72023) and the Leverhulme Foundation.

References

- [1] Arnold V I, Kozlov V V and Neishtadt A I 2006 *Mathematical Aspects of Classical and Celestial Mechanics (Encyclopedia of Mathematical Sciences vol 3)* 3rd edn (Berlin: Springer)
- [2] Bishop A, Forest M, McLaughlin D and Overman E II 1990 A modal representation of chaotic attractors for the driven, damped pendulum chain *Phys. Lett. A* **144** 17–25
- [3] Bolotin S V and Treschev D V 2000 Remarks on the definition of hyperbolic tori of Hamiltonian systems *Regular Chaotic Dyn.* **5** 401–12
- [4] Bolsinov A V and Fomenko A T 2004 *Integrable Hamiltonian Systems Geometry, Topology, Classification* (Boca Raton, FL: Chapman & Hall)
- [5] Bolsinov A V and Oshemkov A A 2006 Singularities of integrable Hamiltonian systems *Topological Methods in the Theory of Integrable Systems* (Cambridge: Cambridge Science Publications) pp 1–67
- [6] Broer H W, Hanssmann H and You J 2005 Bifurcations of normally parabolic tori in hamiltonian systems *Nonlinearity* **18** 1735–69
- [7] Chierchia L and Gallavotti G 1994 Drift and diffusion in phase space *Ann. Inst. H. Poincaré Phys. Théor.* **60** (1) 144
- [8] Delshams A, de la Llave R and Seara T M 2008 Geometric properties of the scattering map of a normally hyperbolic invariant manifold *Adv. Math.* **217** 1096–153
- [9] Elskens Y and Escande D 1991 Slowly pulsating separatrices sweep homoclinic tangles where islands must be small: an extension of classical adiabatic theory *Nonlinearity* **4** 615–67
- [10] Escande D F 1988 Hamiltonian chaos and adiabaticity *Plasma Theory and Nonlinear and Turbulent Processes in Physics, Proc. Int. Workshop (Kiev, Ukraine, 1987)* ed V Bar'yakhtar *et al* (Singapore: World Scientific) pp 398–430
- [11] Fenichel N 1971 Persistence and smoothness of invariant manifolds for flows *Ind. Univ. Math. J.* **21** 193–225
- [12] Fomenko A T 1988 Integrability and nonintegrability in geometry and mechanics *Mathematics and its Applications (Soviet Series)* vol 31 (Dordrecht: Kluwer) (Translated from Russian by M V Tsaplina)
- [13] Fomenko A T (ed) 1991 *Topological Classification of Integrable Systems (Advances in Soviet Mathematics vol 6)* (Providence, RI: American Mathematical Society) (Translated from Russian)
- [14] Gelfreich V 2000 Splitting of a small separatrix loop near the saddle-center bifurcation in area-preserving maps *Physica D* **136** 266–79
- [15] Gelfreich V and Lerman L 2002 Almost invariant elliptic manifold in a singularly perturbed Hamiltonian system *Nonlinearity* **15** 447–57
- [16] Hansmann H 2007 *Local and Semi-Local Bifurcations in Hamiltonian Dynamical Systems (Lecture Notes in Mathematics 1893)* (Berlin: Springer)
- [17] Haller G 1999 Chaos near resonance (*Applied Mathematical Sciences* 138) (New York: Springer)
- [18] Kovacic G and Wiggins S 1992 Orbits homoclinic to resonances, with an application to chaos in a model of the forced and damped sine-Gordon equation *Physica D* **57** 185–225
- [19] Lerman L M and Umanskiy Y L 1998 *Four-dimensional Integrable Hamiltonian Systems with Simple Singular Points (Topological Aspects) (Translations of Mathematical Monographs vol 176)* (Providence, RI: American Mathematical Society) (Translated from the Russian manuscript by A Kononenko and A Semenovich)
- [20] Litvak-Hinenzon A and Rom-Kedar V 2002 Parabolic resonances in 3 degree of freedom near-integrable Hamiltonian systems *Physica D* **164** 213–50
- [21] Litvak-Hinenzon A and Rom-Kedar V 2002 Resonant tori and instabilities in Hamiltonian systems *Nonlinearity* **15** 1149–77
- [22] Litvak-Hinenzon A and Rom-Kedar V 2004 On energy surfaces and the resonance web *SIAM J. Appl. Dyn. Syst.* **3** (4) 525–73
- [23] Neishtadt A I 1984 The separation of motions in systems with rapidly rotating phase *Prikl. Mat. Mekh. USSR* **48** (2) 197–204 (in Russian)
Neishtadt A I 1985 *J. Appl. Math. Mech.* **48** (2) 133–39 (Engl. Transl.)
- [24] Neishtadt A I 1986 Change of an adiabatic invariant at a separatrix *Fiz. Plazmy* **12** (8) 992–1000 (in Russian)
Neishtadt A I 1986 *Sov. J. Plasma Phys.* **12** 568–73 (Engl. Transl.)
- [25] Neishtadt A I 1987 *J. Appl. Math. Mech.* **51** (5) 586–92 (Engl. Transl.)
Neishtadt A I 1987 On the change in the adiabatic invariant on crossing a separatrix in systems with two degrees of freedom *Prikl. Mat. Mekh.* **51** (5) 750–7 (in Russian)
- [26] Neishtadt A 1990 Averaging, capture into resonances, and chaos in nonlinear systems *Chaos Khaos (Woods Hole, MA, 1989)* (New York: American Institute of Physics) pp 261–73
- [27] Neishtadt A, Simó C, Treschev D and Vasiliev A 2008 Periodic orbits and stability islands in chaotic seas created by separatrix crossings in slow-fast systems *Discrete Contin. Dyn. Syst. Ser. B* **10** 621–50

- [28] Neishtadt A and Vasiliev A 2005 Phase change between separatrix crossings in slow-fast Hamiltonian systems *Nonlinearity* **18** 1393–406
- [29] Neishtadt A and Vasiliev A 2007 On the absence of stable periodic orbits in domains of separatrix crossings in nonsymmetric slow-fast Hamiltonian systems *Chaos* **17** 043104
- [30] Neishtadt A I, Sidorenko V V and Treschev D V 1997 Stable periodic motions in the problem on passage through a separatrix *Chaos* **7** 2–11
- [31] Paldor N and Killworth P 1988 Inertial trajectories on a rotating earth *J. Atmos. Sci.* **45** 4013–9
- [32] Radnović M and Rom-Kedar V 2008 Foliations of isoenergy surfaces and singularities of curves *Regular Chaotic Dyn.* **13** 645–68
- [33] Rom-Kedar V 1997 Parabolic resonances and instabilities *Chaos* **7** 148–58
- [34] Rom-Kedar V, Dvorkin Y and Paldor N 1997 Chaotic Hamiltonian dynamics of particle's horizontal motion in the atmosphere *Physica D* **106** 389–431
- [35] Rom-Kedar V and Paldor N 1997 From the tropic to the poles in forty days *Bull. Am. Meteorol. Soc.* **78** 2779–84
- [36] Shlizerman E and Rom-Kedar V 2005 Hierarchy of bifurcations in the truncated and forced nonlinear Schrödinger model *Chaos* **15** (1) 013107 (22pp)
- [37] Litvak-Hinenzon A 2005 The mechanism of parabolic resonance orbits *EQUADIFF 2003, Proc. Int. Conf. Differential Equations (Hasselt, Belgium, 22–26 July 2003)* (Hackensack, NJ: World Sci. Pub.) pp 738–43
- [38] Shlizerman E and Rom-Kedar V 2006 Three types of chaos in the forced nonlinear Schrödinger equation *Phys. Rev. Lett.* **96** 024104
- [39] Shlizerman E and Rom-Kedar V 2009 Classification of solutions of the forced periodic nonlinear Schrödinger equation submitted
- [40] Tennyson J L, Cary J R and Escande D F 1986 Change of the adiabatic invariant due to separatrix crossing *Phys. Rev. Lett.* **56** 2117–20
- [41] Treschev D 2002 Trajectories in a neighbourhood of asymptotic surfaces of a priori unstable Hamiltonian systems *Nonlinearity* **15** 2033–52
- [42] Treschev D 2004 Evolution of slow variables in a priori unstable Hamiltonian systems *Nonlinearity* **17** 1803–41